The middle-late Aalenian event: A precursor of the Mesozoic Marine Revolution

Alicia Fantasia, Emanuela Mattioli, Jorge E. Spangenberg, Thierry Adatte, Enrique Bernárdez, Jorge Ferreira, Nicolas Thibault, François-Nicolas Krencker, Stéphane Bodin

The middle-late Aalenian event: a precursor of the Mesozoic Marine Revolution

Alicia Fantasia[1,2*], Emanuela Mattioli[2,3], Jorge E. Spangenberg[4], Thierry Adatte[5], Enrique Bernárdez[6], Jorge Ferreira[2], Nicolas Thibault[7], François-Nicolas Krencker[1], Stéphane Bodin[1]

[1]*Department of Geoscience, Aarhus University, 8000 Aarhus C, Denmark*

[2]*Univ Lyon, UCBL, ENSL, UJM, CNRS, LGL-TPE, F-69622, Villeurbanne, France*

[3]*Institut Universitaire de France (IUF), Paris Cedex 05, France*

[4]*Institute of Earth Surface Dynamics, University of Lausanne, 1015 Lausanne, Switzerland*

[5]*Institute of Earth Sciences, University of Lausanne, 1015 Lausanne, Switzerland*

[6]*Instituto Superior de Correlación Geológica, Miguel Lillo 205 (CP 4000), San Miguel de Tucumán, Argentina*

[7]*Department of Geosciences and Natural Resource Management, University of Copenhagen, 1350 Copenhagen K, Denmark*

[*]*corresponding author: alicia.fantasia@univ-lyon1.fr*

Abstract

The Aalenian was a time marked by profound environmental and carbon cycle changes. Still, the scarcity of detailed studies hinders a better understanding of the triggering mechanisms and the larger-scale context of Lower to Middle Jurassic environmental perturbations. This study provides an unprecedented high-resolution biostratigraphically well-constrained carbon isotope record ($\delta^{13}C_{org}$ and $\delta^{13}C_{carb}$) for the upper Toarcian–lower Bajocian interval of two expanded limestone-marl alternation successions in France (French Subalpine Basin) and Chile (Andean Basin). The comparison with available records from the Tethyan and Boreal domains highlights that medium-term carbon isotope fluctuations are reproducible across different palaeoceanographic settings from both hemispheres, providing for the first time compelling evidence for recurrent perturbations of the global carbon cycle during the Aalenian. Combined with a review of geological events, climate modes, abundance

and diversity of major fossil groups, and trophic conditions inferred from the calcareous nannofossil record, our study fills the gap in our understanding of global environmental changes in a so-far poorly documented Middle Jurassic stage, intercalated between the early Toarcian Oceanic Anoxic Event and the early Bajocian carbonate crisis. Importantly, this compilation indicates that the Aalenian was a pivotal time interval of environmental perturbations, likely triggering the Mesozoic Marine Revolution.

Keywords: Carbon isotope stratigraphy; Recurrent carbon cycle perturbations; Biotic events; Jurassic

1. Introduction

The Mesozoic was punctuated by several episodes of environmental changes associated with climatic instabilities, severe biotic crises, and perturbations of the global carbon cycle expressed as prominent carbon isotope excursions (CIEs) in marine and terrestrial inorganic and organic materials (e.g., Jenkyns et al., 2002; Dera et al., 2011; Bodin et al., 2015; Korte et al., 2015; Storm et al., 2020). These perturbations were often associated with the development of marine anoxia and the deposition of organic-matter rich strata and are commonly reported as Oceanic Anoxic Events (OAEs, see Jenkyns, 2010 for a review). Over the last decades, the Toarcian-OAE (or T-OAE; e.g., Hesselbo et al., 2000; van Breugel et al., 2006; Suan et al., 2011; Bodin et al., 2016; Xu et al., 2017; Fantasia et al., 2018; Krencker et al., 2020) and the early Bajocian Event (e.g., Suchéras-Marx et al., 2013; Bodin et al., 2017, 2020) have attracted much attention because they represent such episodes of global environmental change associated with large-amplitude CIEs.

The T-OAE was one of the most extreme hyperthermal events of the Mesozoic, likely triggered by intense volcanic activity in the Karoo-Ferrar Province and associated massive release of greenhouse gases into the atmosphere-ocean system (e.g., Courtillot, 1994; Duncan et al., 1997; Pálfy and Smith, 2000; Svensen et al., 2007; Suan et al., 2008). The defining benchmark for the T-OAE is a negative CIE thought to result from the injection of isotopically light volcanogenic, thermogenic, and/or biogenic carbon into the exogenic reservoirs (e.g., Hesselbo et al., 2000; Kemp et al., 2005; McElwain et al., 2005; Cohen et al., 2007; Svensen et al., 2007; Suan et al., 2008; Them et al., 2017; Krencker et al., 2019). The early Bajocian Event is characterized by faunal and floral turnovers in pelagic ecosystems, which may represent part of the Mesozoic Marine Revolution (Vermeij, 1977; Wiggan et al., 2017; Suchéras-Marx et al., 2019; Rojas et al., 2021). These changes are associated with a global carbon cycle perturbation expressed as a positive CIE, thought to reflect elevated rates of organic carbon burial linked to enhanced primary productivity (Bartolini et al., 1999; Jenkyns et al., 2002; Hesselbo et al., 2003; O'Dogherty et al., 2006; Suchéras-Marx et al., 2013; Giraud et al., 2016; Erba et al., 2019; Bodin et al., 2020). Magmatic pulses related to major tectonic rearrangement during the early Middle Jurassic (Bartolini and Larson, 2001; Bill et al., 2001; Labails et al., 2010) have been proposed as a potential trigger of the early Bajocian Event. The injection of CO_2 and/or methane clathrates into the atmosphere may have induced a cascade of environmental feedbacks, including greenhouse conditions, enhanced hydrological cycle and weathering, marine eutrophication, and shallow water carbonate production crisis (e.g., Suchéras-Marx et al., 2015; Bodin et al., 2017).

Bracketed in between the Toarcian and the Bajocian, the Aalenian has received much less attention, although it was likely a time of environmental instabilities marked by carbon cycle perturbations and marine biotic turnovers (e.g., O'Dogherty et al., 2006; Sandoval et al., 2008; Gómez et al., 2009). Hence, some important information can be gained from this

bridging time interval to put the T-OAE and early Bajocian Event into a broader context and better understand global carbon cycle dynamics during the Mesozoic.

Here, we present a high-resolution biostratigraphic (calcareous nannofossils), sedimentological and geochemical (stable carbon isotopes, Rock-Eval pyrolysis) study of two expanded successions, namely Le Brusquet (French Subalpine Basin, SE France) and Agua de la Falda (Andean Basin, N Chile). These successions were previously dated by ammonite faunas and spanned the upper Toarcian–lower Bajocian interval. The main objective of this paper is to assess the potential causal links between the carbon isotope perturbations and palaeoenvironmental changes significantly affecting the carbonate factory, as depicted from various inorganic, organic, and biotic proxies. Specifically, this study provides (i) detailed carbon isotope records of bulk organic matter and carbonates, (ii) a correlation of the studied sections with coeval sites using nannofossil biostratigraphy and carbon isotope stratigraphy, and (iii) an evaluation of the stratigraphic reproducibility of the carbon isotope variations and an appraisal of the influence of local processes on the global signal.

2. Geological setting

Le Brusquet and Agua de la Falda localities offer extended and continuously exposed strata of upper Toarcian–lower Bajocian age and include both the Toarcian/Aalenian and the Aalenian/Bajocian boundaries, according to previously established ammonite biozones (Le Brusquet: Mouterde et al., 1966; Caloo, 1970; de Graciansky et al., 1993; Agua de la Falda: von Hillebrandt and Schmidt-Effing, 1981; Marticorena and Tapia, 1982). The successions are composed of marly limestone-marl alternations, deposited in the French Subalpine Basin and the Andean Basin, respectively (Fig. 1).

The development of the French Subalpine Basin began during the Middle to Late Triassic (e.g., de Graciansky et al., 1993; Razin et al., 1996; Mariotti et al., 2012). During the Middle Jurassic, the basin was a transitional zone between the epicontinental sea of the Paris Basin and the deeper Ligurian Tethys, along the NW margin of the Tethys (Fig. 1; Ferry and Rubino, 1989; Thierry, 2000). The Le Brusquet succession is now exposed in SE France (Fig. 1), ~10 km NE of the town of Digne-les-Bains along the Bouinenc stream and the D22 road linking the villages of Marcoux and Draix (GPS coordinates, base of the section: 44°08'10.07''N; 06°18'14.19''E). In the studied area, Middle Jurassic sedimentary successions were covered by at least 3 km of Upper Jurassic to Eocene sedimentary deposits and are part of the Digne thrust sheets, which overthrusted autochthon strata towards the SW (Gidon and Pairis, 1992; Lickorish and Ford, 1998). The Le Brusquet succession was buried under ca. 3 km overburden (Haccard et al., 1989) and was likely impacted by burial diagenesis and complex tectonic history. These transformations are also suggested by the degree of organic matter maturation (oil window-beginning of gas window stage; Levert, 1989) of Middle Jurassic deposits in the Digne area.

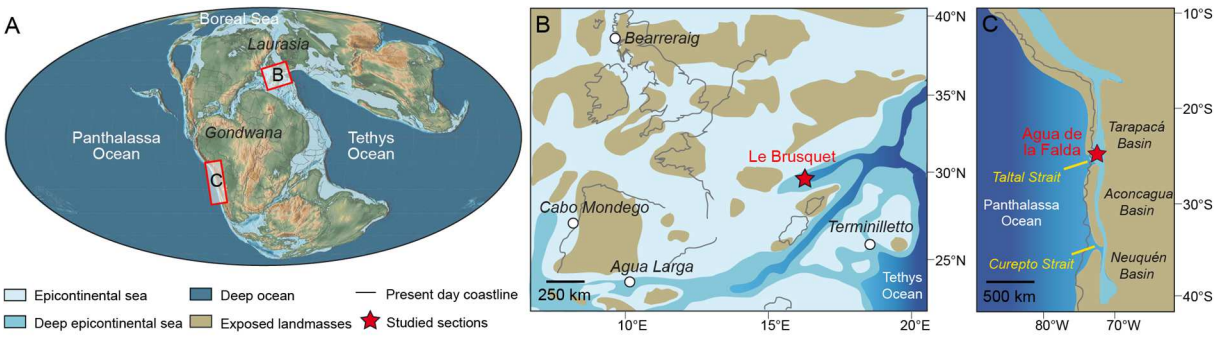

Fig. 1 : (A) Global Middle Jurassic palaeogeographic reconstruction (after Scotese, 2014), with the location of the French Subalpine (B) and Andean (C) basins. **(B)** Palaeogeographic map of the western Tethys (after Thierry, 2000) with the location of Le Brusquet section (French Subalpine Basin, France) and other comparative key sites discussed in the text: Cabo Mondego (Lusitanian Basin, Portugal), Agua Larga (Subbetic Basin, Spain), Bearreraig (Hebrides Basin, the United Kingdom), and Terminilletto (Umbria-Marche Basin, Italy). Note that the central Tethys was not yet open during the Aalenian. **(C)** Palaeogeographic map of the Andean Basin, which was divided into the Tarapacá, Aconcagua and Neuquén subbasins. The location of the Agua de la Falda section and the position of the communicating straits with the Panthalassa Ocean are shown.

123 The Andean Basin was an elongated back-arc basin along the SW Gondwana margin,
124 which developed in response to extensional and/or transtensional tectonics related to the
125 subduction of the proto-Pacific plate and the formation of the Andean magmatic arc during
126 the Jurassic and Early Cretaceous (Uliana et al., 1989; Vicente, 2005; Charrier et al., 2007).
127 Despite the development of the volcanic arc to the west, a connection with Panthalassa Ocean
128 was likely possible through marine connecting straits during the Middle Jurassic (Gröschke et
129 al., 1988; Prinz et al., 1994). The Agua de la Falda succession is exposed in N Chile (Fig. 1),
130 near the Potrerillos locality in the Atacama Region (GPS coordinates: 26°30'34.03''S;
131 69°20'34.5''W). The succession was likely not too strongly affected by burial diagenesis and
132 eventually by the tectonic history related to the formation of the Andean Cordillera since this
133 was not the case for older deposits of Toarcian age in the same area (Fantasia et al., 2018).

134

135 **3. Material and methods**

136 *3.1. Sampling*

137 Le Brusquet and Agua de la Falda sections were measured and sampled for
138 geochemical analyses with a vertical resolution of 45–90 cm and 5–20 cm, respectively. In
139 parallel, the lithology, sedimentary features, fossil content, and ichnofossil associations were
140 described for each level sampled. The samples showing clear evidence of diagenetic
141 neoformed, recrystallized calcite, or containing macroscopic allochems were avoided. About
142 10–20 g of macroscopically homogeneous sample were selected, dried at 45°C, crushed, and
143 powdered using an agate mortar at the Department of Geoscience, Aarhus University prior to
144 analysis.

145

3.2. Calcareous nannofossil biostratigraphy

Smear slides for calcareous nannofossil identification were prepared at the LGL-TPE, Université Claude Bernard Lyon 1. A total of 76 samples from Le Brusquet and 20 from the Agua de la Falda were selected at regular space intervals in the marl-limestone alternations. A small amount of crushed rock was mixed with water before spreading onto a cover slide (Bown and Young, 1998). Cover slides were then mounted onto the microscope slide using Rhodopass B resin (polyvinyl acetate). Sample slides were then studied using a Leica DM750P optical microscope at 1000x magnification. Two transverses of the slide (12.8 mm^2) were scanned and the encountered nannofossils were counted. The slides were further analysed to recover rare species. The preservation state of the nannofossils was evaluated based on etching and overgrowth of the specimens, using the preservation index and criteria proposed by Roth (1994).

3.3. Carbon and oxygen isotopes

Carbon and oxygen isotope compositions ($\delta^{13}C_{carb}$ and $\delta^{18}O_{carb}$, ‰ VPDB) of aliquots of powdered whole-rock samples (Le Brusquet: n= 395, Agua de la Falda: n=41) were determined using a Thermo Fisher Scientific (Bremen Germany) Gas Bench II connected to a Delta Plus XL isotope mass spectrometer at the Institute of Earth Surface Dynamics of the University of Lausanne (IDYST–UNIL). The measured $\delta^{13}C_{carb}$ and $\delta^{18}O_{carb}$ values were normalized to VPDB scale using reference laboratory standard (Carrara Marble, $\delta^{13}C$ = +2.05‰, $\delta^{18}O$ = –1.7‰) and international reference materials NBS18 carbonatite ($\delta^{13}C$ = –5.01‰, $\delta^{18}O$ = –23.01‰) and NBS19 limestone ($\delta^{13}C$ = +1.95‰, $\delta^{18}O$ = –2.2‰). Analytical uncertainty (1σ) monitored by replicate analyses of the laboratory standard Carrara Marble was not greater than ±0.05‰ for $\delta^{13}C$ and ±0.1‰ for $\delta^{18}O$.

Carbon isotope compositions of bulk organic matter ($\delta^{13}C_{org}$, ‰ VPDB) were determined on decarbonated (treatment with 10% HCl) powdered whole-rock samples (Le Brusquet: *n*= 689, Agua de la Falda: *n*= 303) by using an elemental analyser Carlo Erba 1108 connected to a Thermo Fisher Scientific Delta V Plus isotope ratio mass spectrometer at IDYST–UNIL. The repeatability and intermediate precision of the $\delta^{13}C_{org}$ values were better than 0.05‰.

3.4. Rock-Eval pyrolysis

Total organic carbon (TOC, wt.%) content, mineral carbon (MinC, wt.%) content, hydrogen index (HI, mg HC/g TOC, HC=hydrocarbons), oxygen index (OI, mg CO_2/g TOC), and T_{max} (°C) were measured on powdered whole-rock samples (Le Brusquet: n= 639, Agua de la Falda: n= 298) using a Rock-Eval 6 (Espitalié, 1985; Behar et al., 2001) at the Institute of Earth Sciences of the University of Lausanne (ISTE–UNIL). Measurements were calibrated using the IFP160000 standard. T_{max} estimates of the thermal maturation level of the organic matter (Espitalié et al., 1977; Peters, 1986). HI values were not interpreted for TOC ≤0.2 wt.%, and T_{max} values were rejected when S_2 ≤0.3 mg HC/g avoiding misinterpretation of flat thermograms (Peters, 1986). The parameter Q_{carb}= 7.976*MinC (Jiang et al., 2017) was used to estimate the proportion of carbonate with MinC values as the sum of mineral carbon obtained during pyrolysis and oxidation phases (Lafargue et al., 1998).

4. Results

4.1. Lithological description and biostratigraphy

4.1.1. Le Brusquet

193 The upper Toarcian–lower Bajocian at Le Brusquet is about 400 m-thick and
194 dominated by dm- to m-thick alternations of offshore marl and marly limestone (Fig. 2). The
195 succession shows relatively monotonous lithology and is expanded compared to previously
196 documented contemporaneous European sections (Fig. 3; e.g., Sandoval et al., 2008; Gomez
197 et al., 2009; Price, 2010; Korte et al. 2015). The lithostratigraphy and ammonite
198 biostratigraphy of equivalent successions in Le Brusquet area have been previously described
199 by Mouterde et al. (1966), Caloo (1970) and de Graciansky et al. (1993), and the following
200 ammonite zones have been recognised: Aalensis (late Toarcian), Opalinum (early Aalenian),
201 Murchisonae (middle Aalenian), Concavum (late Aalenian), and Discites (early Bajocian).
202 The ammonite biostratigraphy is complemented here by nannofossil data (Fig. 3). The base of
203 the succession is dominated by dark grey marl, intercalated with few yellowish lenticular,
204 nodular, dm-thick limestone beds (Fig. 2A), assigned to the uppermost Toarcian (Aalensis
205 zone). The transition towards the Aalenian is marked by a progressive evolution to rhythmic
206 marly limestone-marl alternations (Fig. 2A). The lower Aalenian (Opalinum zone) is
207 composed of marly limestone-dominated rhythmic alternations, with few dm-thick lenticular
208 limestone beds at the base. A 5 cm-thick brown clayey layer is intercalated at 80 m. The
209 middle Aalenian (Murchisonae zone) is composed of massive marly limestone-marl rhythmic
210 alternations (Fig. 2B), with the limestone becoming progressively thinner and more marly
211 towards the top of the interval. The upper Aalenian (Concavum zone) shows marl with
212 rhythmic intercalations of thin marly limestone beds (Fig. 2C). The lower Bajocian (Discites
213 zone) is composed of marl, which grades into regular limestone-marl alternations (Fig. 2C).
214
215
216

Fig. 2 : **(A)** Representative field photographs of Le Brusquet (A–C) and Agua de la Falda (D–G) sections. **(A)** The Upper Toarcian–lower Aalenian transition is marked by an evolution from marl-dominated to limestone-dominated deposits. **(B)** The middle Aalenian is composed of limestone-marl rhythmic alternations. **(C)** The upper Aalenian shows marl with rhythmic intercalations of thin marly limestone beds, which grades into regular marl and limestone alternations in the lower Bajocian. **(D)** The upper Toarcian–lower Bajocian–Bathonian–(?) Callovian shows an alternation of marl and limestone. **(E)** Close-up view of the lower Aalenian marl (sometimes finely laminated)-limestone alternations. **(F)** Close-up view of the limestone marker bed at 26 m, which is almost entirely composed of oysters. **(G)** The upper Aalenian–Bajocian transition is marked by a limestone bed with bivalve concentrations (red arrows). The top of the bed, representing the unconformity between the lowermost Bajocian and the Bathonian–(?) Callovian, is a hard ground with borings (dashed lines) infilled with phosphatic clasts from the phosphorite conglomerate bed. This bed is the basis of a Bathonian–(?) Callovian succession composed of silicified limestone.

232 *4.1.2. Agua de la Falda*

233 The Agua de la Falda locality in the Potrerillos area was selected because it presents
234 one of the most expanded and well-exposed upper Toarcian–lower Bajocian succession in
235 Chile, offering a globally-distributed insight of the environmental conditions. It is composed
236 of a 52 m-thick alternation of marl and marly limestone (Fig. 2). The Agua de la Falda
237 outcrop belt can be followed laterally to the Quebrada El Asiento section (~2.5 km away from
238 Agua de la Falda), which was previously described for its lithostratigraphy and ammonite
239 biostratigraphy (von Hillebrandt and Schmidt-Effing 1981; Marticorena and Tapia 1982;
240 Perez 1982). In addition, the T-OAE interval has been identified further down in the
241 succession (Fantasia et al., 2018), bracketing the stratigraphic framework of the studied
242 succession. The ammonite biostratigraphy is based on the scheme developed for the Andean
243 regions and correlated with the European Standard Ammonite zones (von Hillebrandt and
244 Schmidt-Effing, 1981; von Hillebrandt and Westermann, 1985; Riccardi, 2008). Specifically,
245 the following ammonite assemblage zones were distinguished in the Potrerillos area: (i)
246 *Pleydellia* cf. *fluitans* (~Aalensis), (ii) *Bredyia manflasensis* (~Opalinum), (iii) *Zurcheria*
247 *groeberi* (~Murchisonae), (iv) *Puchenquia malarguensis* (~Concavum), (v) horizon of
248 *Podagrosiceras maubeugei* (~Aalenian/Bajocian boundary). *Pseudotoites* cf. *sphaeroceroides*
249 indicates the lowermost Bajocian, (vi) (?) *Xenocephalites* sp. and (?) *Epistrenoceras* sp. of
250 late Bathonian to Callovian age (von Hillebrandt and Westermann, 1985).

251 The base of the section (Aalensis zone, upper Toarcian) is composed of wavy to
252 nodular marly limestone beds, rarely bioclastic, alternating with thin marl interbeds. Those
253 alternations grade up-section into a dark brown marl-dominated interval, which contains
254 limestone nodules and large ammonites (unidentifiable, ~30 cm diameter) and alternates with
255 nodular marly limestone beds. The marl-dominated interval is overlain by massive dm-thick
256 bioclastic limestone beds, equivalent to the beds 8 described by von Hillebrandt and Schmidt-

Effing (1981) at the Toarcian–Aalenian transition. The rest of the succession is dominated by wavy to nodular, bioclastic (wackestone to packstone), bioturbated, marly limestone beds, which alternate with dark brown, organic-matter rich, thin-bedded to laminated, marls (Fig. 2E). The marls contain limestone nodules and mm-scale phosphatic peloids. Several firm grounds are present. The macrofossil content in the bioclastic limestones consists of bivalves (mostly oysters), brachiopods (mostly terebratulids), crinoids, ammonites, and scarce belemnites and gastropods. The shells are poorly sorted, wholly or almost entirely fragmented, and are oriented along cross bedding, or are normally graded. At 26 m, a 60 cm-thick normally-graded limestone bed with an erosive base and almost composed by articulated oysters (*Lopha* sp.), is a marker bed in the studied succession (Fig. 2F). This coquina bed is equivalent to bed 12 described by von Hillebrandt and Schmidt-Effing (1981), which is assigned to a middle–late Aalenian age (Murchisonae–Concavum zones). The limestone and marl become silty to sandy from 40 m upwards, and the proportion of marl relative to limestone increases. The silty marl-dominated interval is capped by a 20 cm-thick erosive-based limestone bed including thin-shelled bivalves accumulated in distinct layers (Fig. 2G). The upper part of the limestone bed presents borings filled with phosphatic clasts. This is overlain by a cm-thick phosphorite conglomerate bed (Fig. 2G), laterally discontinuous with an erosive base containing heterometric, sub-angular to rounded, poorly sorted phosphate clasts (Fig. 2G). The limestone bed below the conglomerate corresponds to bed 16 described by von Hillebrandt and Schmidt-Effing (1981), which was assigned to an early Bajocian age. The conglomerate of early Bajocian age is disconformably overlain by silicified limestone (Fig. 2G), with ripple laminations, of late Bathonian–(?) Callovian age described as bed 17 by von Hillebrandt and Schmidt-Effing, 1981. Most of the Bajocian interval is hence largely condensed and/or missing, and marked by reworked deposits.

282 *4.2. Calcareous nannofossils*

283 At Le Brusquet, calcareous nannofossils were identified in 76 samples throughout the
284 upper Toarcian–lower Bajocian interval providing a suite of biostratigraphic events (see
285 Supplementary Information and Fig. S1), whereas the analysed samples at Agua de la Falda
286 were all barren. At Le Brusquet, the dominant calcareous nannofossil taxa are represented by
287 *Schizosphaerella*, Biscutaceae (including various species of *Similiscutum, Biscutum* and
288 *Discorhabdus*), several species of *Lotharingius*, *Watznaueria* with a cross structure in the
289 central area (namely: *W. colacicchii*, *W. contracta*, and *Watznaueria* aff. *W. contracta*),
290 *Watznaueria* with a bridge in the central area (*W. communis* and several morphotypes of *W.*
291 *britannica* defined in Giraud et al., 2006), and *Watznaueria* without structures in the central
292 area (*W. fossacincta* and *Watznaueria* aff. *W. manivitiae*; Fig. 3). The assemblage
293 composition shows important variations across the Aalenian (Fig. 4). The base and
294 intermediate, carbonate-rich part of the succession (Aalensis to middle Murchisonae zones;
295 upper Toarcian to middle Aalenian) are characterized by the lowest nannofossil content and
296 by the dominance in nannofossil assemblage of *Schizosphaerella* spp. (an *incertae sedis*,
297 commonly considered to be a dinoflagellate cyst; Bown, 1987). The coccolith fraction,
298 although very rare, is dominated by Biscutaceae, with a peak at around 140–160 m
299 (Murchisonae zone; middle Aalenian), while *Lotharingius* coccoliths show an inverse trend.
300 However, being the dominant coccolith forms, such inverse trend in Biscutaceae and
301 *Lotharingius* can be due to the closed-sum effect. The carbonate-rich interval also bears
302 micrometre-sized plant debris commonly observed in the smear slides. A sudden change in
303 the assemblage composition is observed from ~220 m up to the top of the section (middle
304 Murchisonae to Discites zones; middle Aalenian to lower Bajocian), where nannofossil
305 amounts progressively increased and *Watznaueria* spp. became dominant. In particular, this

306 shift to *Watznaueria* spp. dominance is driven by elevated proportions (20 to 50%) of those
307 forms bearing a cross structure in the central area.

308

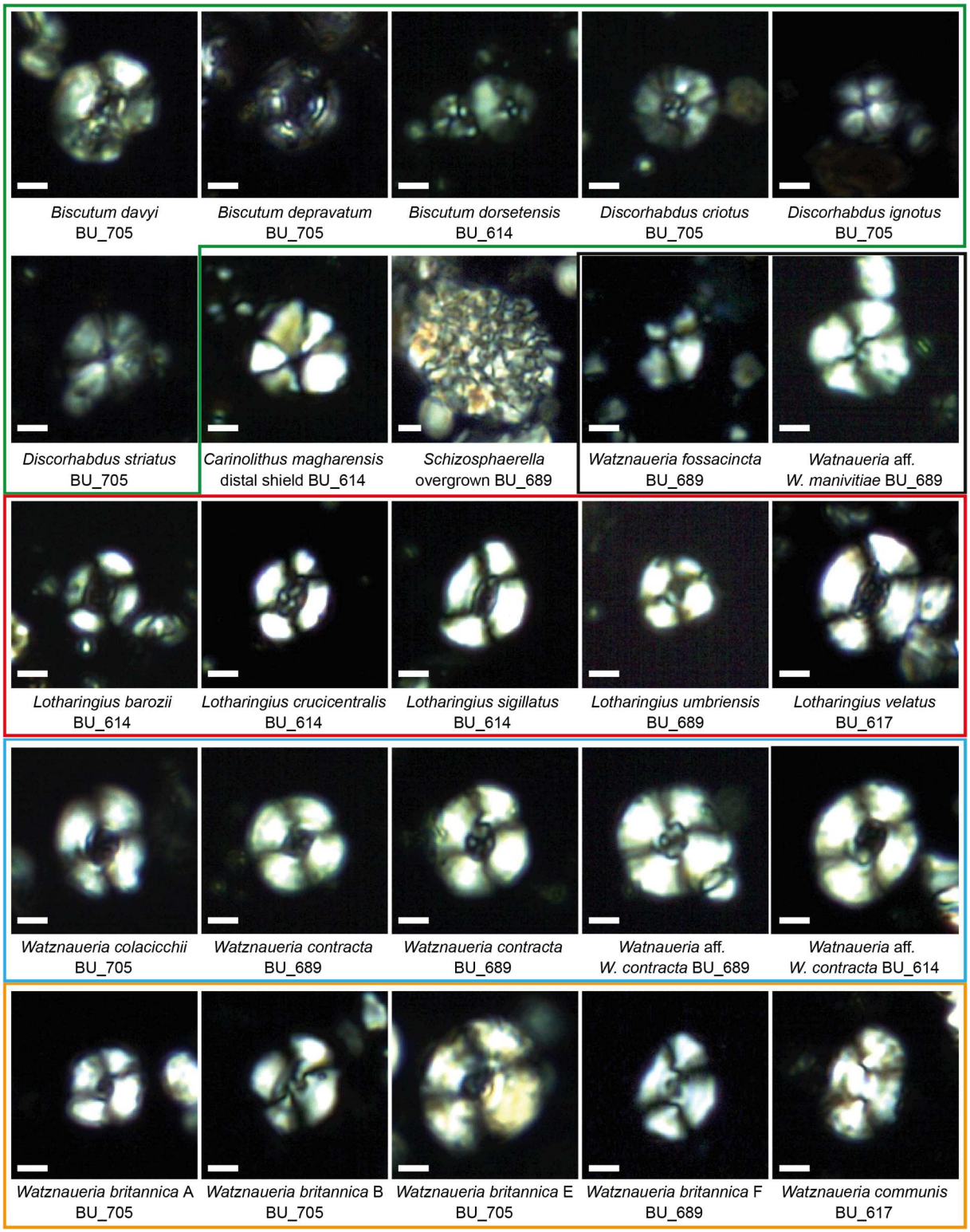

Fig. 3 : Micrographs of representative calcareous nannofossils from Le Brusquet section, under cross-polarized light. The colour code refers to the dominant taxa shown in Figure 5: Biscutaceae (green), *Lotharingius* (red), *Watznaueria* with a cross structure in the central area, (blue), *Watznaueria* with a bridge in the central area (orange), and *Watznaueria* without stuctures (black).

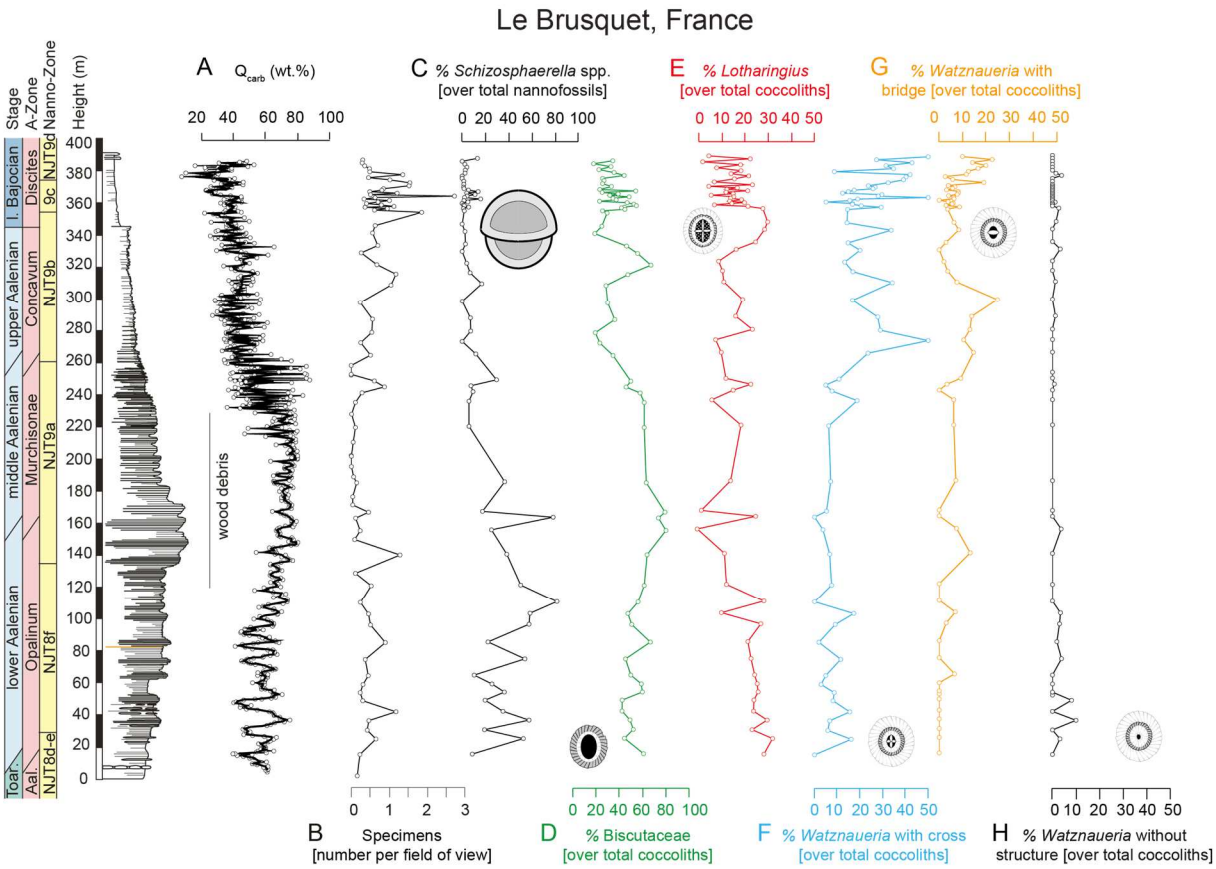

315

316 **Fig. 4:** **(A)** Carbonate content (Q_{carb}) for Le Brusquet section is shown next to **(B)** the calcareous nannofossil abundances,
317 and the percentages of the dominant taxa, i.e., **(C)** *Schizosphaerella*, **(D)** Biscutaceae, **(E)** *Lotharingius,* **(F)** *Watznaueria*
318 with a cross structure in the central area, **(G)** *Watznaueria* with a bridge in the central area, and **(H)** *Watznaueria* without
319 structures. Note the significant increase in *Watznaueria* across the middle–late Aalenian. Wood debris are particularly present
320 in the middle Aalenian.

321

322 *4.3. Organic matter and carbonate contents*

323 *4.3.1. Le Brusquet*

324 At Le Brusquet, TOC contents are comprised between 0.1 and 1.0 wt.%, with
325 maximum values in the Aalensis and Opalinum zones (Fig. 5). The TOC values are high
326 (average 0.7 wt.%) up to the Opalinum–Murchisonae zonal transition before gradually
327 decreasing up to the lower Murchisonae zone. This is followed by a scattered increase of the
328 TOC in the upper Murchisonae zone, with values up to 0.8 wt.% in the marl and minimum
329 values of 0.1 wt.% in the limestone. This is followed by steady TOC contents up to the top of

the section, with values fluctuating around 0.5 wt.%. HI (2–87 mg HC g^{-1} TOC; average 21 mg HC g^{-1} TOC) and OI (18–284 mg CO_2 g^{-1} TOC; average 61 mg CO_2 g^{-1} TOC) values are relatively low throughout the section (Fig. 5), with the highest HI and lowest OI recorded from the Aalensis zone up to the lower Murchisonae zone. This is followed by a decrease of the HI and generally higher OI (≤ 284 mg CO_2 g^{-1} TOC) up to the top of the section. The T_{max} values are uniform within 494–498 °C. Q_{carb} values fluctuate between 7.8 and 87.3 wt.% and broadly mirror TOC values, with a long-term increasing trend from the base of the section up to the Murchisonae–Concavum zonal transition. This gradual increase in Q_{carb} values is expressed as a change to more massive marly limestone-marl rhythmic alternations. This is followed by a decrease in the Concavum zone and relatively steady values up to the top of the section (Fig. 5).

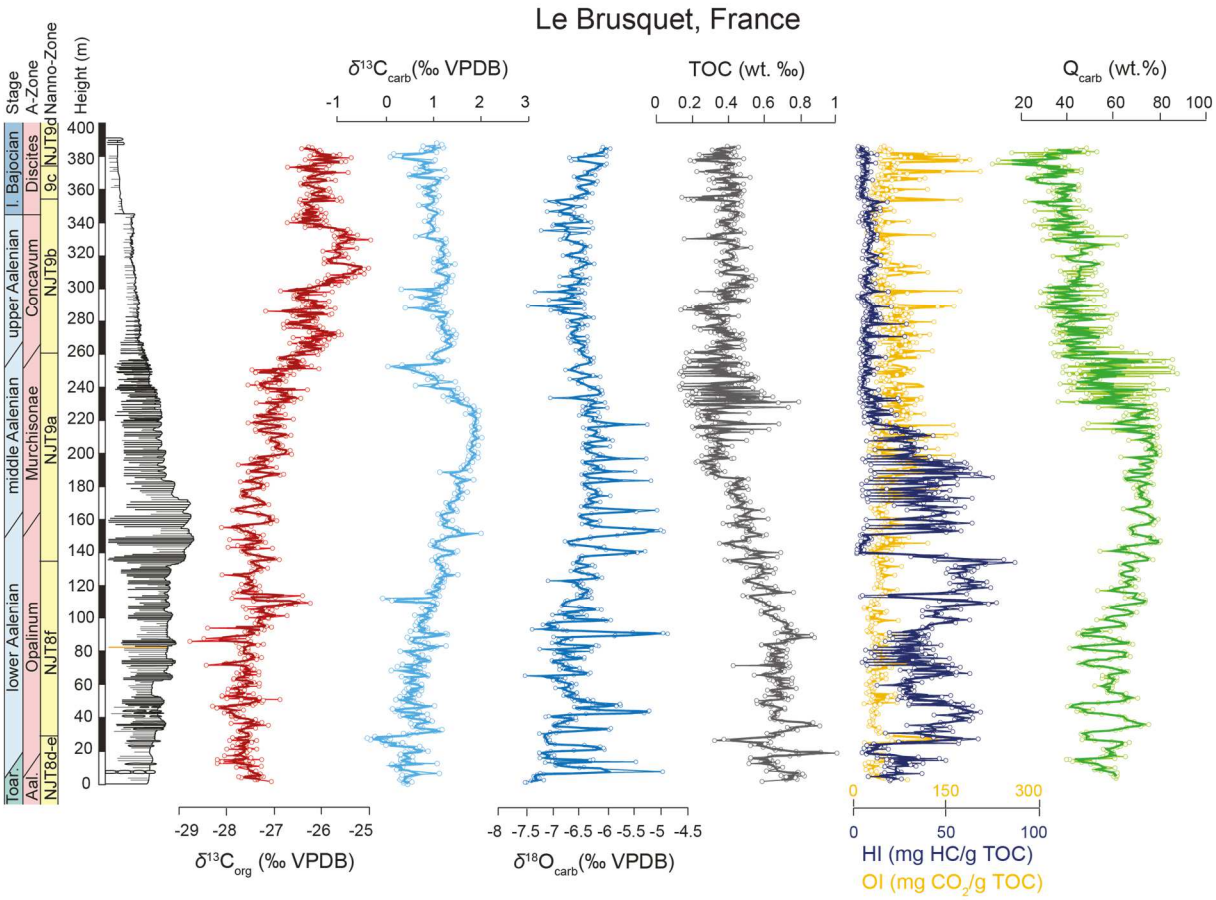

Fig. 5: Isotopic composition ($\delta^{13}C_{org}$, $\delta^{13}C_{carb}$, $\delta^{18}O_{carb}$), total organic carbon (TOC) content, hydrogen index (HI), oxygen index (OI), and carbonate content (Q_{carb}) at Le Brusquet. The trend lines correspond to a 4-points moving average.

4.3.2. Agua de la Falda

At Agua de la Falda, TOC content is generally higher than at Le Brusquet, with values up to 1.9 wt.% (Fig. 6).

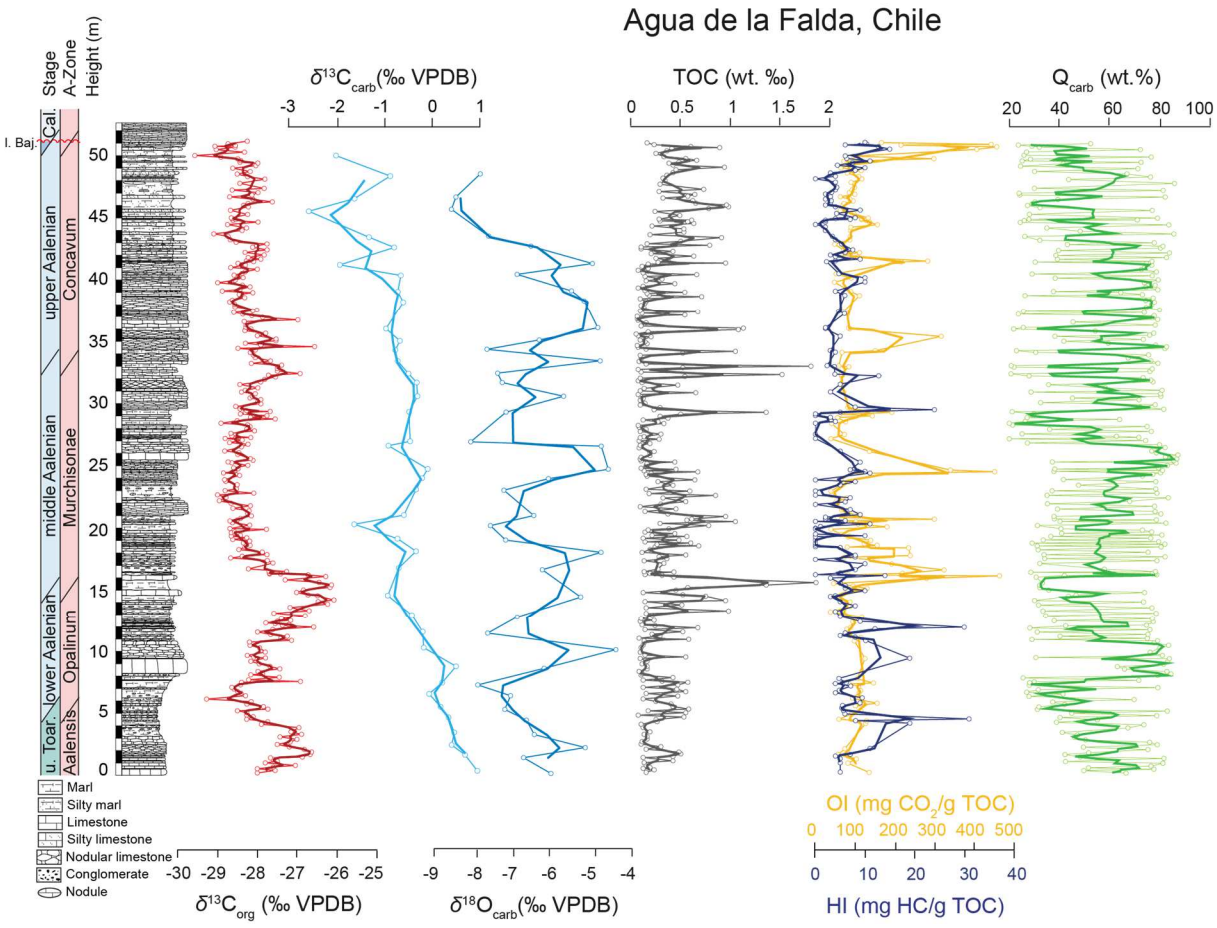

Fig. 6: Isotopic composition ($\delta^{13}C_{org}$, $\delta^{13}C_{carb}$, $\delta^{18}O_{carb}$), total organic carbon (TOC) content, hydrogen index (HI), oxygen index (OI), and carbonate content (Q_{carb}) at Agua de la Falda. The trend lines correspond to a 4-points moving average.

A gradual increase is recorded up to the Opalinum–Murchisonae zonal transition, with a maximum of 1.9 wt.% in the laminated marl. This is followed by a decrease at the base of the Murchisonae zone and a slight increase up to the middle Murchisonae zone. This trend is followed by a gradual decrease of the TOC values up to the upper Murchisonae zone, and

356 then a scattered increase across the Murchisonae–Concavum zonal transition. TOC values
357 show a general increase in the Concavum zone, followed by a decreasing trend near the
358 Bajocian–Bathonian–(?) Callovian disconformity surface. HI values are generally low (≤ 31
359 mg HC g^{-1} TOC; average 6 mg HC g^{-1} TOC), whereas OI values are moderately high (≤ 449
360 mg CO_2 g^{-1} TOC; average 116 mg CO_2 g^{-1} TOC), and both index fluctuate throughout the
361 section (Fig. 6). Q_{carb} values vary between 0.2 and 83.8 wt.%, and show a high scatter which
362 refects the alternation between marl and limestone. Three intervals of decreasing Q_{carb} values
363 are recorded at the Toarcian/Aalenian boundary, in the Opalinum zone, in the upper
364 Murchisonae zone, and in the Concavum zone, respectively (Fig. 6).

365

366 *4.4. Carbon and oxygen isotopes*

367 *4.4.1. Le Brusquet*

368 At Le Brusquet, the $\delta^{13}C_{org}$ values range between –29.9 and –24.9‰ (Figs. 5 and 7)
369 and show a long-term gradual increase of about 3.0‰ from the upper Toarcian to the
370 uppermost Aalenian, which culminates with maximum values in the Concavum zone. Distinct
371 $\delta^{13}C_{org}$ medium-term fluctuations are superimposed on this long-term positive trend. The
372 $\delta^{13}C_{org}$ profile shows a ~1‰ negative excursion near the Toarcian/Aalenian boundary,
373 followed by a ~1‰ increase in the Opalinum zone, reaching values up to –26‰ with a first
374 maximum in the upper Opalinum zone. Two distinct ~1.5‰ negative shifts are recorded at the
375 Opalinum–Murchisonae zonal transition and in the Murchisonae zone, followed by an
376 increase in $\delta^{13}C_{org}$ values reaching –25.5‰ at the Murchisonae–Concavum zonal transition.
377 The $\delta^{13}C_{org}$ shows two ~1.0–1.5‰ negative shifts in the Concavum zone that interrupt a
378 progressive increase to a maximum value of –24.9‰. The Aalenian/Bajocian boundary is
379 marked by a decrease in $\delta^{13}C_{org}$ (Fig. 5).

The $\delta^{13}C_{carb}$ values vary between –0.5 and 2.0‰ (Fig. 5) and show a general increasing trend from the Aalensis zone up to the middle Murchisonae zone, which mimics the increase of carbonate content in the section. The increasing trend is followed by a shift to more negative $\delta^{13}C_{carb}$ in the upper part of the section, where the lithology changes toward marl-dominated deposits. The $\delta^{18}O_{carb}$ values fluctuate between –7.5 and –1.7‰ (Fig. 5), displaying broadly a similar trend as the $\delta^{13}C_{carb}$ values.

4.4.2. Agua de la Falda

At Agua de la Falda, $\delta^{13}C_{org}$ values range between –29.6 and –25.1‰, with consecutive medium-term shifts of ~1.0–2.5‰ magnitude (Figs. 6 and 7). The $\delta^{13}C_{org}$ profile shows a ~2‰ negative shift at the Toarcian/Aalenian boundary, followed by an increase of up to –26‰ at the Opalinum–Murchisonae zonal transition, associated with high TOC. The Murchisonae zone shows a broad stepped ~2.5‰ negative $\delta^{13}C_{org}$ shift, followed by an increase to a maximum value of –27‰ near the Murchisonae–Concavum zonal transition, coupled with an increase in TOC. The $\delta^{13}C_{org}$ values show two ~1.5‰ negative shifts in the lower Concavum zone and a decrease near the Aalenian/Bajocian boundary. These negative shifts are followed by a marked increase to the maximum value of –25.1‰ below the lower Bajocian–Bathonian–(?) Callovian disconformity surface (Fig. 6).

The $\delta^{13}C_{carb}$ values fluctuate between –3.3 and 1.0‰ (Fig. 6) and show a long-term decreasing trend throughout the section, interrupted by more positive values across the Murchisonae–Concavum zonal transition. The $\delta^{18}O_{carb}$ values fluctuate between –8.6 and –4.3‰ (Fig. 6).

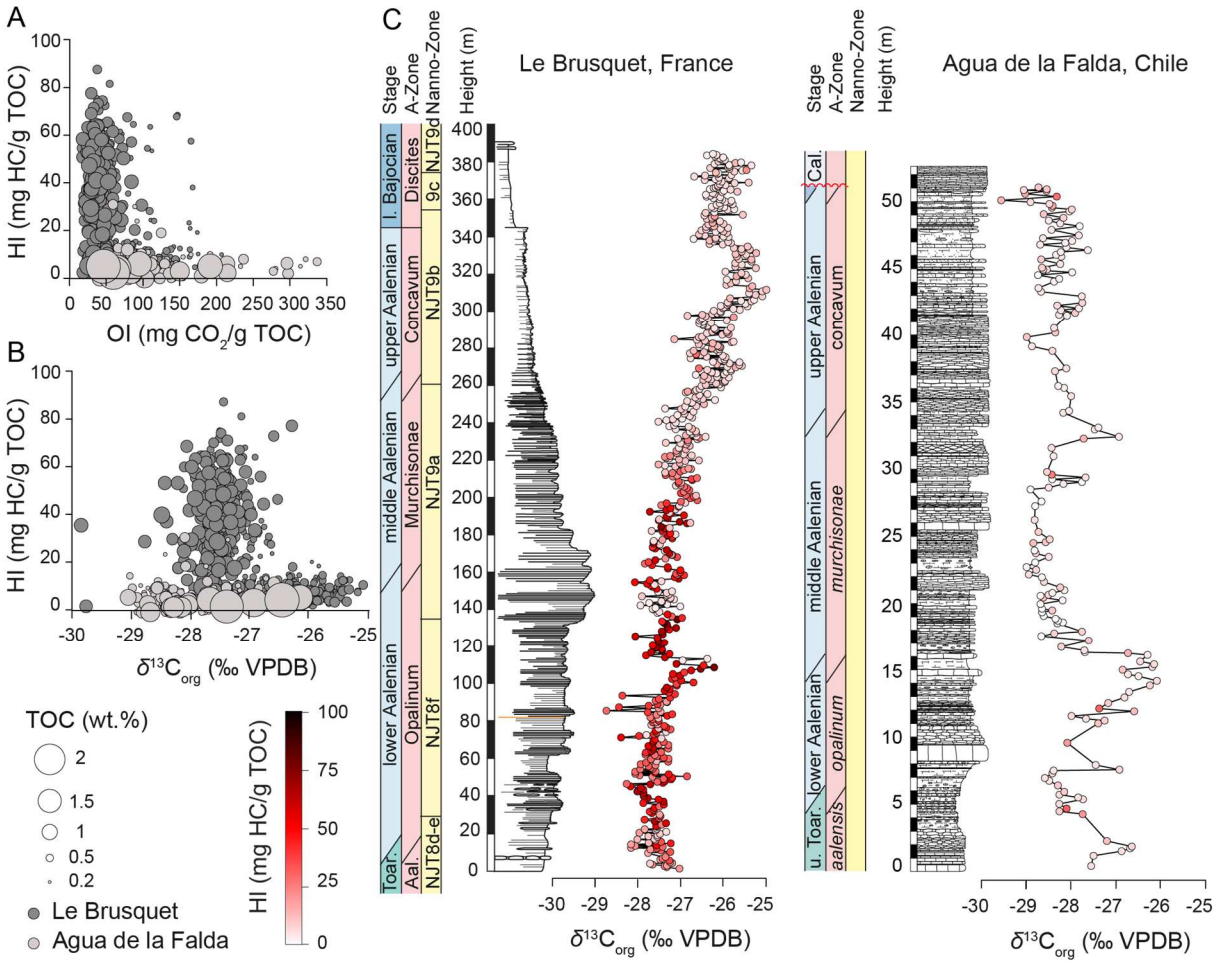

Fig. 7: **(A)** Scatterplot of the hydrogen index (HI) versus the oxygen index (OI) in relation with the total organic carbon (TOC) content for Le Brusquet and Agua de la Falda sections. **(B)** Relationship between $\delta^{13}C_{org}$ and hydrogen index for Le Brusquet and Agua de la Falda sections. **(C)** Bulk organic matter isotopic composition ($\delta^{13}C_{org}$) for Le Brusquet and Agua de la Falda sections, compared to the stratigraphic evolution of the hydrogen index (HI) values. Note the absence of clear relationship between the type/preservation of the organic matter and the $\delta^{13}C_{org}$ trend.

5. Discussion

5.1. Calcareous nannofossils

5.1.1. Biostratigraphic constraints

The chronostratigraphic frame and age assignment provided by ammonites for Le Brusquet section (Caloo, 1970; de Graciansky et al. 1993) is confirmed by our new calcareous nannofossil biostratigraphy (Fig. S1). In particular, the occurrence of *W. contracta* and *C.*

magharensis approximate the Toarcian/Aalenian boundary, which correlates to the base of the NJT8 zone of the Ferreira et al. (2019) biochronological scheme (also used in the GTS 2020). The middle Aalenian was identified by the consecutive FOs of *W. britannica* morphotype A and *W. communis* (NJT9a zone). The Aalenian/Bajocian boundary and basal Bajocian were recognised by the FO of *R. escaigii* and the LCO of small *Similiscutum* (NJT9c zone).

Calcareous nannofossil data are also available for the Agua Larga (Spain, Sandoval et al., 2008) and Terminilletto (Italy, Baumgartner et al., 1995) sections, where whole-rock $\delta^{13}C_{carb}$ have been measured (Aguado et al., 2008; Sandoval et al., 2008; Morettini et al., 2002). The nannofossil and carbon isotope data of these sections were compared with the new dataset from Le Brusquet and Agua de la Falda (Fig. 8). To ensure accurate comparisons with the studied sections, nannofossil data from Terminilletto (studied by one of us, EM) and from Agua Larga (Aguado et al., 2008) were reconsidered in the light of recently published taxonomic revision (see the synthesis in Ferreira et al., 2019). In particular, the specimen of *W. contracta* shown by Aguado et al. (2008; figure 5-39) is larger than 7 µm; thus it should be considered as a *W.* aff. *W. contracta* according to Tiraboschi and Erba (2010). Aguado et al. (2008) reported a sharp increase in proportions of *W. contracta* in the Agua Larga section from 59.40 m. After reconsideration, this increase may instead correspond to the inception of *W.* aff. *W. contracta*. If so, the record of the Agua Larga section is consistent with that of Le Brusquet (Fig. 8). Likewise, the specimens of *W. britannica* shown by Aguado et al. (2008; figure 5-44) might correspond to a transitional form close to *W. manivitiae*. We hence added the FO of *W.* aff. *W. manivitiae* as an alternative to the FO of *W. britannica* reported by Aguado et al., 2008 (Fig. 8).

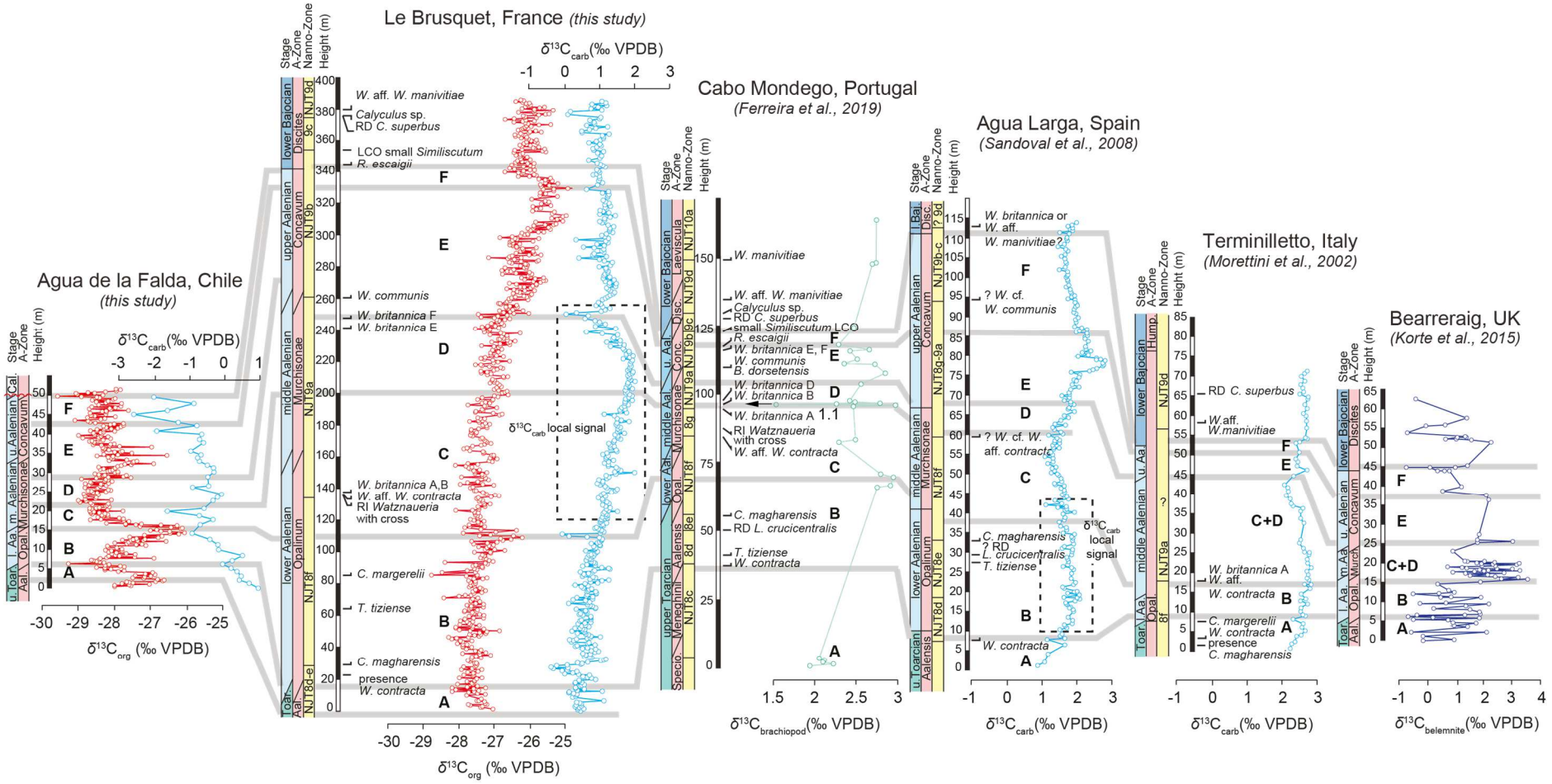

Fig. 8: High-resolution carbon isotope records ($\delta^{13}C_{org}$, $\delta^{13}C_{carb}$) of the upper Toarcian–lower Bajocian interval of Le Brusquet and Agua de la Falda sections, and comparison with available key records from the European area: Cabo Mondego, Lusitanian Basin, Portugal (Ferreira et al., 2019); Agua Larga, Subbetic Basin, Spain (Sandoval et al., 2008); Terminilletto, Umbria-Marche Basin, Italy (Morettini et al., 2002); Bearreraig, Hebrides Basin, the United Kingdom (Korte et al., 2015). Note that the grey lines correspond to correlations proposed in this study, based on biostratigraphy and chemostratigraphy and highlights carbon isotope shifts (intervals A–F) that can be correlated between the different sites from the Panthalassa, and Tethyan and Boreal realms. At Le Brusquet and Agua Larga, the box with dashed line indicates the interval where the $\delta^{13}C_{carb}$ signal is likely influenced by the carbonate ooze exported from adjacent platforms.

445 The comparison between nannofossil events at Le Brusquet, Agua Larga, and
446 Terminilletto shows that some events can be traced across the three sections (Fig. 8). The
447 nannofossil record of Agua Larga and Terminilletto allows a tentative application of the
448 nannofossil zones of Ferreira et al. (2019) that provides correlation with Le Brusquet record
449 (Fig. 8). In particular, the occurrence of *W. contracta* is relatively consistent between the three
450 sections, and similarly to Le Brusquet, *W.* aff. *W. contracta* and *W. britannica* A occur close
451 to each other at Terminilletto. According to our stable isotope and biostratigraphic data, the
452 FO of *W.* aff. *W. manivitiae* is consistent between the three sections and further allow
453 potential recognition of subzone NJT9d despite the lack of observation of the LO of
454 *Calyculus* spp. at Agua Larga and Terminilletto (Fig. 8).

455

456 *5.1.2. Palaeoenvironmental implications*

457 Although calcareous nannofossils are very rare at Le Brusquet (Fig. 5), the percentage
458 of the dominant taxa can be interpreted in terms of palaeoenvironmental changes, especially
459 in the carbonate-rich part of the section between 130 and 220 m. Calcareous nannofossil
460 abundances (Fig. 4B) provide raw information on the general trends. The Aalensis to
461 Opalinum zones (upper Toarcian to lower Aalenian, 0–130 m) display moderate values of
462 nannofossil abundances along with relatively high percentages of shallow-dweller taxa,
463 proliferating either in times of relative oligotrophy (such as *Schizosphaerella* spp.; Fig. 4C) or
464 meso-eutrophic conditions of surface waters (such as Biscutaceae and *Lotharingius* spp.; Fig.
465 4D–E). *Schizosphaerella* was likely better adapted to overall oligotrophic conditions in
466 shallow-waters, where nutrients were probably recycled in times of intensified storms
467 (Mattioli and Pittet, 2004; Aguado et al., 2008; Reggiani et al., 2010). However, some authors
468 (Claps et al., 1995; Erba, 2004; Tremolada et al., 2005) interpreted *Schizosphaerella* as a

469 deep-dweller taxon, proliferating in time of surface-water oligotrophy. Biscutaceae are
470 commonly associated with eutrophic environments both in the Jurassic and in the Cretaceous,
471 thrivring in high-fertility surface-waters (Roth and Bowdler, 1981; Premoli Silva et al., 1989;
472 Watkins, 1989; Erba, 1992; Mattioli and Pittet, 2004; Tremolada et al., 2006; Mattioli et al.,
473 2008). *Lotharingius* probably dwelled in shallow-waters and was adapted to moderately high
474 nutrient concentrations (Pittet and Mattioli, 2002; Mattioli and Pittet, 2004; Olivier et al.,
475 2004; Tremolada et al., 2005; Mattioli et al., 2008). Overall, calcareous nannofossil
476 assemblage at the base of the Le Brusquet section can be considered as indicative of
477 alternating high- and low-fertility conditions in surface waters.

478 The Opalinum to middle Murchisonae zones (lower to middle Aalenian, ~130–220 m)
479 is marked by the lowest relative abundances in nannofossils, decreasing proportions of
480 *Schizosphaerella* spp. and low percentages of *Lotharingius* spp., whereas Biscutaceae show
481 the highest values (Fig. 4C–E). Moreover, this interval also corresponds to the most
482 carbonate-rich part of the succession and with the highest concentration in micrometer-sized
483 wood debris observed in smear slides (Fig. 4). Such observations may suggest either
484 increased continental runoff and bio-limiting elements input to epicontinental basins or
485 relative proximity from source areas at times of platform progradation. Whatever the cause,
486 the observed dominance of Biscutaceae may have been triggered by enhanced continent-
487 derived nutrient input.

488 The dominant features observed in the middle Murchisonae to Discites zones (middle
489 Aalenian to lower Bajocian, ~220–400 m) comprise the overall decreasing trend in
490 Biscutaceae proportions and the progressive and prominent increase in *Watznaueria* bearing a
491 cross in its central area (Fig. 4D and F). This trend encompasses an increase in *Watznaueria*
492 bearing a bridge in the central area (Fig. 4G), which were likely opportunistic forms,
493 proliferating in times of global eutrophication related to major oceanic reorganisation (Giraud

et al., 2016). Alternatively, they may have developed the ability to bloom in nutrient-rich environments previously unexploited by other species (Suchéras-Marx et al., 2015). Likewise, major changes have been documented in the siliceous microplankton, with a major radiolarian turnover across the middle–late Aalenian (Yao, 1997; Bartolini et al., 1999; Aguado et al., 2009). This faunal change has been interpreted as the biological response to palaeotectonic rearrangements in the Western Tethys linked to the central Atlantic spreading, which likely induced palaeoceanographic modifications, with global ocean chemistry changes and eutrophication (e.g., Aguado et al., 2008; Sandoval et al., 2008).

5.2. Effects of diagenesis and different carbonate phases on the isotope records

The potential diagenetic overprint on the marly limestone-marl alternations was evaluated at Le Brusquet and Agua de la Falda to assess if the $\delta^{13}C_{carb}$ and $\delta^{18}O_{carb}$ data could be used as primary environmental indicators. Diagenetic processes on pelagic carbonates generally have less influence on the carbon isotopes than oxygen isotopes (e.g., Schrag et al., 1995). The organic matter mineralization releases ^{13}C-depleted dissolved inorganic carbon (DIC). Therefore, recrystallization-neomorphism of carbonate phases during burial diagenesis will lower the $\delta^{13}C_{carb}$ values (e.g., Weissert et al., 1979; Marshall, 1992; Schrag et al., 1995). Actually, Le Brusquet section is composed of micrite-rich deposits, which are less prone to diagenetic fluid migration and carbon buffered. At Le Brusquet, the moderate correlation between $\delta^{13}C_{carb}$ and Q_{carb} values (r=0.45, $p<0.001$) suggests a relationship between the whole-rock carbonate content and the carbon isotope composition. The long-term marine carbon isotope record is mainly governed by changes in the organic carbon fluxes relative to the total carbon in the different carbon pools (e.g., Berner, 1987). Long-term $\delta^{13}C_{carb}$ records can however potentially be influenced by regional carbon cycling processes. These include

518 the incorporation of carbonate particles with varying carbon isotope compositions exported
519 from platforms and pelagic mud (e.g., Swart and Eberli, 2005; Godet et al., 2006; Bodin et al.,
520 2016). It has however been demonstrated that the contribution of nannofossil carbonate to the
521 global oceanic carbon cycle is negligible during the Middle Jurassic (Suchéraz-Marx et al.,
522 2012) and hence did likely not significantly contribute to the $\delta^{13}C_{carb}$ record of Le Brusquet.
523 Long-term fluctuations in the contribution of riverine DIC fluxes to the ocean can also induce
524 shifts in the $\delta^{13}C_{carb}$ and $\delta^{18}O_{carb}$ profiles (e.g., Kump and Arthur, 1999; Kemp et al., 2020),
525 which are decoupled from global changes in the carbon cycle. Given the difference between
526 the carbon isotope record from Le Brusquet and other European sites, it is hence not excluded
527 that the $\delta^{13}C_{carb}$ profile from Le Brusquet likely do not solely reflect changes in the global
528 carbon cycle but also the superimposed influence of local carbon cycling
529 processes.Furthermore, in the studied area, Middle Jurassic sedimentary successions were
530 covered by at least 3 km of Jurassic to Eocene sediments and underwent a complex regional
531 alpine tectonic history (Digne Nappe; Levert, 1989; Lickorish and Ford, 1998), pointing to the
532 influence of burial diagenesis on the deposits. At Le Brusquet, the relationship between
533 $\delta^{13}C_{carb}$ and $\delta^{18}O_{carb}$ values (r=0.57, $p<0.001$) together with generally low $\delta^{18}O_{carb}$ values
534 suggest a significant overprint of burial diagenesis, precluding the use of the $\delta^{18}O_{carb}$ as a
535 reliable environmental proxy. The influence of burial diagenesis is further supported by high
536 T_{max} values (494–498°C), which indicate mature organic matter (gas window; Espitalié et al.,
537 1985).

538 At Agua de la Falda, the correlation between $\delta^{13}C_{carb}$ and $\delta^{18}O_{carb}$ values is very weak
539 (r=0.19, p=0.12), suggesting that burial diagenesis had no significant influence on the carbon
540 isotope values. This low diagenetic overprint is also supported by the lack of correlation
541 between $\delta^{13}C_{carb}$ and Q_{carb} values (r=0.18, p=0.11). Nonetheless, the long-term negative
542 $\delta^{13}C_{carb}$ trend is paralleled by a lithological transition towards the shallowest facies observed

throughout the succession and the increasing proportion of detrital material. This suggests that diagenetic processes, including organic matter oxidation and incorporation of ^{13}C-depleted carbon and/or changes in the relative content of carbonate ooze, may have driven the negative $\delta^{13}C_{carb}$ trend without any link with the global signal. Interpretation of $\delta^{18}O_{carb}$ values is excluded from the discussion since they are particularly low, suggesting diagenetic overprint related to dissolution and recrystallization-neomorphism (Schrag et al., 1995). The absence of S_2 peak hampers any reliable interpretation of T_{max} values and the influence of thermal diagenesis.

5.3. Evaluation of the degree of preservation of the organic matter

At Le Brusquet, burial diagenesis impacted the type of preserved organic matter. The more refractory terrestrial organic matter was likely preferentially preserved during burial diagenesis than the labile marine organic matter (e.g., de Lange et al., 1994; Arndt et al., 2013). Low HI and OI values (averages 21 mg HC g^{-1} TOC and 61 mg CO_2 g^{-1} TOC, respectively; Fig. 5) and high T_{max} values (494–498°C) well within the gas window point to overmature organic matter in these rocks. This high thermal maturity prevented the assessment of the organic matter type in the HI *vs*. OI plot (Fig. 7A). Although a minor contribution of overmature phytoplankton-derived marine organic matter can not be excluded, the occurrence of microscopic and macroscopic fossil wood particles (e.g., between 130-220 m) suggests a predominance of terrestrial organic matter, likely conveyed to the French Subalpine Basin from the surrounding emerged landmasses such as the Massif Central. At Agua de la Falda, the source of the preserved organic matter is difficult to assess because it has been overprinted by diagenetic processes (S_2< 0.3 mg HC/g and therefore not reliable T_{max} values). The absence of smectite in the Pliensbachian–Toarcian interval from the same area

(Fantasia et al., 2018) confirms that burial diagenesis affected the deposits. However, this overprint was likely not too strong in the studied area as indicated by the presence of kaolinite (Fantasia et al., 2018), which supports higher thermal burial than smectite before transformation into illite or chlorite (e.g., Burtner and Warner, 1986; Chamley, 1989).

Nonetheless, although the studied successions underwent diagenetic overprint related to the complex diagenetic and tectonic history of the studied areas, similar medium-term shifts and range of $\delta^{13}C_{org}$ values were recorded at both sites, suggesting that the carbon isotope composition of the preserved organic matter may not have been strongly modified. Furthermore, the isotope composition of the kerogen is generally preserved from low thermal maturation degrees until relatively high degree of metamorphism (e.g., McKirdy and Powell, 1974; Schoell, 1984; Spangenberg and Macko, 1998) No high thermal gradients were reached at Le Brusquet and Agua de la Falda, supporting the use of the $\delta^{13}C_{org}$ as an environmental signal. Additionally, the absence of a relationship between the preservation of the organic matter type (HI values) and the $\delta^{13}C_{org}$ values at both localities (Fig. 7) sustained the organic carbon isotope records a an environmental proxy.

5.4. Recurrent global carbon cycle disturbances across the Aalenian

The Aalenian carbon isotope stratigraphy was hitherto derived from $\delta^{13}C$ records of whole-rock carbonates and biogenic calcite from Tethyan and Boreal sites (Spain: Sandoval et al., 2008; Gómez et al., 2009, Italy: Morettini et al., 2002, United Kingdom: Jenkyns, 2002; Price et al., 2010; Korte et al., 2015, Portugal: Ferreira et al., 2015, 2019, Morocco: Krencker et al., 2014). Besides the Agua Larga succession in Spain, which is presently the most expanded high-resolution $\delta^{13}C_{carb}$ record for the upper Toarcian–lower Bajocian interval, the other records generally present low resolution data, restricted to short stratigraphic intervals,

591 and/or poor biostratigraphic constraints. Based on the correspondence between the different
592 Tethyan and Boreal records, it has been suggested that some of the $\delta^{13}C_{carb}$ shifts may relate
593 to supraregional controls (e.g., Price, 2010; Sandoval et al., 2008). Nonetheless, records from
594 outside the Tethyan and Boreal domains and derived from organic matter were inexistent
595 before our study leaving large uncertainties about the global extent of the carbon cycle
596 perturbations and about triggering mechanisms.

597 Comparing our $\delta^{13}C$ records and published datasets highlights that similar medium-
598 term $\delta^{13}C$ patterns are shared between sites from both hemispheres. However, the interplay
599 between global and local processes on the long-term carbon isotope signal varies between
600 palaeoceanographic settings. Consecutive medium-term shifts can indeed be compared across
601 Tethyan, Boreal, and Panthalassic sites (Fig. 8), providing compelling evidence that recurrent
602 global carbon cycle perturbations occurred during the Aalenian. The Le Brusquet carbon
603 isotope record not only depicts several medium-term shifts that were previously identified in
604 Tethyan and Boral sites (e.g., Price, 2010; Sandoval et 2008) but also other undescribed
605 fluctuations. Hence, the Aalenian $\delta^{13}C$ record appears much more complex than previously
606 thought as our results allow identifying seven intervals (A to F; Fig. 8) of global carbon cycle
607 perturbations.

608 At Le Brusquet, the uppermost Toarcian is marked by a negative shift (interval A) in
609 the $\delta^{13}C_{org}$ and $\delta^{13}C_{carb}$ values, reaching the lowest values at the Toarcian/Aalenian boundary.
610 This trend is also observed in Chile at Agua de la Falda. This negative carbon isotope shift
611 was previously identified in the $\delta^{13}C_{carb}$ records of hemipelagic carbonates and marine
612 biogenic carbonates at different sites from the Tethyan and Boreal realms (Spain: Sandoval et
613 al., 2008; Portugal: Ferreira et al., 2019; Italy: Morettini et al., 2002; United Kingdom: Price,
614 2010; Korte et al., 2015; France: Harazim et al., 2013; Morocco: Krencker et al., 2014). The

615 lower Aalenian (Opalinum zone) is marked by positive shifts in $\delta^{13}C_{org}$ and $\delta^{13}C_{carb}$ (interval
616 B) at Le Brusquet and at Agua de la Falda and were previously identified in carbonates from
617 Tethyan and Boreal sites (Price et al., 2010; Sandoval et al., 2008). The lower–middle
618 Aalenian transition (Opalinum–Murchisonae zonal transition) from Le Brusquet is marked by
619 a negative $\delta^{13}C_{org}$ excursion (interval C) which was not observed in the $\delta^{13}C_{carb}$ record.
620 Nonetheless, a negative $\delta^{13}C_{carb}$ excursion marked the Opalinum–Murchisonae transition at
621 Agua Larga in Spain (Sandoval et al., 2008), suggesting that local conditions may have
622 modulated the $\delta^{13}C_{carb}$ record at Le Brusquet. Indeed, interval C at Le Brusquet shows the
623 highest carbonate content associated with more massive marly limestone-marl rhythmic
624 alternations (Fig. 5), suggesting that material exported from neritic environments may have
625 shifted the $\delta^{13}C_{carb}$ record towards more positive values. Hence, the influence of local
626 conditions related to different amounts of carbonate ooze exported from adjacent platforms
627 may explain differences between the $\delta^{13}C_{carb}$ profiles from Le Brusquet and Agua Larga (e.g.,
628 Swart and Eberli, 2005; Godet et al., 2006; Bodin et al., 2016) (Fig. 8). Alternatively, a
629 change in the organic matter type and/or preservation may explain differences between the
630 organic and inorganic records. However, the absence of a relationship between HI and $\delta^{13}C_{org}$
631 values suggests that the $\delta^{13}C_{org}$ trend reflects a genuine supraregional/global signal. This
632 interpretation is likely supported by a similar decrease in $\delta^{13}C$ values in the bulk carbonate
633 from Spain, belemnites from the United Kingdom and brachiopod shells from Portugal (Fig.
634 8, interval C). At Le Brusquet, the Murchisonae zone (interval D) is marked by a distinct
635 negative shift in the $\delta^{13}C_{org}$. A similar trend can be identified in Chile at Agua de la Falda, but
636 it is more difficult to trace in the less expanded successions (Fig. 8).

637 Notably, at Le Brusquet the Murchisonae–Concavum zonal transition (middle–late
638 Aalenian) is associated with a marked positive $\delta^{13}C$ trend (interval E) which can be identified

639 in both carbonates and organic matter. This is followed by a negative carbon isotope
640 excursion across the Aalenian/Bajocian boundary (interval F) and then a return to less
641 negative $\delta^{13}C$ values in the early Bajocian. These negative and positive excursions are
642 traceable in both organic matter and carbonates across the different sites from the Tethys,
643 Boreal domain, and Panthalassa (Fig. 9) and were previously identified as reflecting global
644 events (e.g., Spain: O'Dogherty et al., 2006; Sandoval et al., 2008; Gomez et al., 2009,
645 France: Corbin, 1994; Suchéras-Marx et al., 2013, Italy: Morettini et al., 2002; United
646 Kingdom: Jenkyns et al., 2002; Hesselbo et al., 2003; Price, 2010, Morocco: Bodin et al.,
647 2020).

648 The dataset from Le Brusquet and Agua de la Falda highlights for the first time the
649 occurrence of recurrent perturbations of the global carbon cycle during the Aalenian.
650 Although the long-term $\delta^{13}C$ trend seems to be influenced by local processes across the
651 Aalenian, medium-term shifts (intervals A–F) are reproducible between different
652 palaeogeographic settings in both hemispheres. Therefore, these shifts reflect synchronous
653 changes in the organic and carbonates carbon and calls for the implication of global driving
654 mechanisms.

655

656 *5.5. Aalenian environmental perturbations*

657 The evolution of environmental conditions across the Aalenian has been so far
658 undervaluated compared to early Toarcian and early Bajocian events. However, evidences of
659 climatic and environmental changes during the Aalenian (Fig. 9) indicate that it might
660 represent a key time interval to better understand the wider context and environmental
661 feedback mechanisms surrounding such major events.

Our results suggest that environmental changes occurred across the middle–late Aalenian. At Le Brusquet, a general increase in carbonate content associated with a decrease in calcareous nannofossil abundances is recorded across the middle Aalenian (Murchisonae zone; Fig. 7). A similar pattern was recorded in contemporaneous hemipelagic settings from Portugal (Ferreira et al., 2019) and Spain (Sandoval et al., 2008). Hence, the evolution of carbonate content at Le Brusquet likely represents a supraregional trend and reflects the intensity of carbonate production and export from surroundings platforms. The middle Aalenian was likely a time of high carbonate export into basinal settings from the Tethyan realm during a relative sea level fall (Hardenbol et al., 1998; Jacquin et al., 1998). A relative sea-level fall during the middle Aalenian has been inferred from the presence of unconformities and development of prograding shallow platform sediments in most Western Tethyan sites during this time interval and has been related to the Mid-Cimmerian tectonic uplift (de Graciansky et al., 1993; Durlet and Thierry, 2000; Léonide et al., 2007). Middle Aalenian platform environments surrounding the French Subalpin Basin (e.g., Beaujolais, Provence and Grands Causses subbasins) and other Tethyan sites (e.g., Bulgaria, Saudi Arabia, France, Germany) were marked by abrupt lithological changes such as the deposition of bioclastic (crinoids, brachiopods, sponges) calcarenititic limestone (Elmi and Rulleau, 1993; Ciszak et al., 1996; Rousselle, 2001; Floquet 2000), iron-rich oolithic limestones (e.g., Ohmert et al., 1996; Rulleau et al., 2001), or hiatuses (Metodiev, 1997; Le Nindre et al., 1990; Delfaud et al., 2000). Such changes in the sedimentation style during the middle Aalenian in platform settings point out to the initiation of a deterioration in environmental conditions. Importantly, these changes in the platform carbonate factory and pelagic carbonate producers correspond to the onset of a positive carbon isotope trend in bulk organic matter and bulk and brachiopod carbonate in contemporaneous Tethyan sites (Fig.9; Portugal, Spain, France).

686 Severe palaeoenvironmental changes are recorded during the middle–late Aalenian
687 (Murchisonae–Concavum zonal transition) as attested by the sharp decrease in carbonate
688 content at Le Brusquet and in other contemporaneous successions from France, Portugal, and
689 Spain, where the highest calcareous nannofossil abundances are observed. In
690 contemporaneous platform settings from the Tethyan area, peculiar sedimentation unknown in
691 earlier sequences have been reported as thin-shelled bivalve buildups (Spain: Molina et al.,
692 2018), siliceous sponge mud-mounds (Portugal: Duarte et al., 2001; France: Floquet et al.,
693 2000; 2012), iron-rich oolithic limestones (Switzerland: Lauper et al., 2021), and hiatuses
694 and/or condensed/reduced deposits (Arabia Saoudia: Le Nindre et al., 1990; Bulgaria:
695 Metodiev, 1997; France: Delfaud et al., 2000; Rousselle, 2001; Germany: Ohmert et al.,
696 1996). Such lithological changes in different palaeogeographic settings indicate a
697 supraregional event of carbonate factory demise. The relative sea-level rise recorded during
698 the late Aalenian in almost all series of Western Europe (de Graciansky et al., 1998; Durlet
699 and Thierry, 2000) likely participated in the deterioration of neritic carbonate factory (e.g.,
700 Gabilly et al., 1985; Léonide et al., 2007). Nonetheless, biotic changes (Fig. 9) indicate that
701 besides local factors, global changes in water mass circulation and chemistry across the
702 middle–late Aalenian may have played a key role in driving the environmental changes.
703 Specifically, this time interval saw the emergence of *Watznaueria*, in particular the forms
704 with a cross spanning the central area, which will dominate up to the early Bajocian (Fig. 9;
705 this study; Suchéras-Marx et al., 2015; Giraud et al., 2016). These forms have been
706 interpreted as opportunistic, proliferating in times of environmental instability related to
707 enhanced nutrient concentrations or temperature changes (Giraud et al., 2016). The genus
708 *Watznaueria* as a whole was in fact very sensitive to paleoceanographic and paleoclimatic
709 changes across the Aalenian/Bajocian boundary and the rise of these forms is likely related to
710 the increase in carrying capacity in the photic zone (Suchéras-Marx et al., 2015). The

supraregional increase in *Watznaueria* also coincides locally with the dominance of Biscutaceae (Sandoval et al., 2008; Aguado et al., 2009), generally also interpreted as eutrophic forms developing in nutrient-rich surface waters (e.g., Roth and Bowdler, 1981; Mattioli and Pittet, 2004; Tremolada et al., 2006). The concomitant emergence of *Watznaueria* in different Tethyan sites (Fig. 9; Portugal, Spain, France) testifies to a global change towards eutrophic conditions in the oceanic domain, whereas the presence of Biscutaceae most likely relates to local conditions specific to each basin (Fig. 9). There is compelling evidence that the Aalenian was a time of palaeoenvironmental changes, biotic reorganisation and carbon cycle perturbation. The development of eutrophic conditions during the middle Aalenian combined to relative sea-level variations likely triggered the intiation of environmental changes while the most severe changes occurred across the late Aalenian. Indeed, our results suggest that this time interval was marked by the demise of platform carbonate factories associated to an increase in eutrophic calcareous nannofossils (genus *Watznaueria*) which are concomitant with the most positive carbon isotope values. The middle–upper Aalenian positive $\delta^{13}C$ excursion may hence reflect increasing productivity in sea-surface waters as previously suggested (Sandoval et al., 2008) and a carbonate productivity crisis. This middle–late Aalenian event certainly represents a precursor episode of environmental changes prior to the early Bajocian event. The increase in TOC coupled to the positive $\delta^{13}C_{org}$ values recorded at Le Brusquet and Agua de la Falda across the middle–upper Aalenian can hence be interpreted as the record of increased marine primary productivity and/or enhanced organic matter burial.

The early Middle Jurassic was a critical time interval of evolutionary and ecological changes (Fig. 9; Table 1), major tectonic rearrangement, and major changes in Mesozoic oceanic current patterns. A shift from a Toarcian warm mode to an Aalenian cold mode has been suggested based on a compilation of oxygen isotope data (Korte et al., 2015). Though

736 the climatic evolution is still poorly documented across the Aalenian, rising seawater
737 temperatures have been deduced from oxygen isotopes of belemnites from Spain (Gomez et
738 al., 2009). However, the lack of supporting data hampers to evaluate the global or local extent
739 of this middle Aalenian warming event and to assess its causal mechanisms. The
740 coccolithophorid event presented in this study coincides with other important biotic changes
741 in other planktonic groups in worldwide distributed sites (e.g., Wiggan et al., 2017). Indeed, a
742 dinoflagellate turnover has been reported across the Aalenian, and radiolarians have a quasi-
743 completely replaced the Early Jurassic fauna (Yao, 1997; Sandoval et al., 2008).

744 Interestingly, the revolution in planktonic biota coincides with the diversification of
745 planktivorous fish (Friedman et al., 2010; Guinot and Cavin, 2016) and cephalopods, together
746 with the extinction of Early Jurassic ammonite taxa and their replacement by families that
747 dominated throughout the Middle Jurassic (Fig. 9; Sandoval et al., 2001; O'Dogherty et al.,
748 2006; Wiggan et al., 2018). Conversely, within other nekton, a crisis has been documented in
749 belemnites (Dera et al., 2016). Moreover, bivalves, brachiopods, bryozoans, and benthic
750 foraminifera also underwent evolutionary changes across the Aalenian (Hallam, 1976;
751 Alméras and Fauré, 2000; Taylor and Ernst, 2008; Canales and Henriques, 2008; Gómez et
752 al., 2009). Hence, the change observed in planktonic groups across the middle–late Aalenian
753 likely triggered a reorganisation of the entire food chain. Our study provides compelling
754 evidence for biotic and environmental changes in both pelagic and neritic environments at a
755 supraregional scale, pointing out to a middle–late Aalenian event. So far, the lower Bajocian
756 event has been seen as the most extreme episode of environmental changes in the Middle
757 Jurassic, with a major carbonate crisis and a shift to biogenic silica production and
758 sedimentation (Bartolini et al., 1996; 1999; Cobianchi et al., 2002; Gorican et al., 2012;
759 Giraud et al., 2016). However, our study indicates that palaeoceanographic,
760 palaeoenvironmental, and palaeoecological changes occurred already earlier, and that the

761 middle–late Aalenian event may hence represent a precursor to the early Bajocian event,
762 initiating the Mesozoic Marine Revolution. Although establishing a precise correspondence
763 between the onset of volcanic activity and environmental changes remains to date elusive, one
764 cannot exclude that magmatic pulses may have started earlier than previously thought, i.e.,
765 before the early Bajocian. Indeed, evidence of global warming, major biotic and carbon cycle
766 changes during the middle–late Aalenian suggests a similar cascade of environmental
767 feedbacks driven by volcanism known from other Mesozoic events (e.g., Caruthers et al.,
768 2013; Bond and Wignall, 2014).

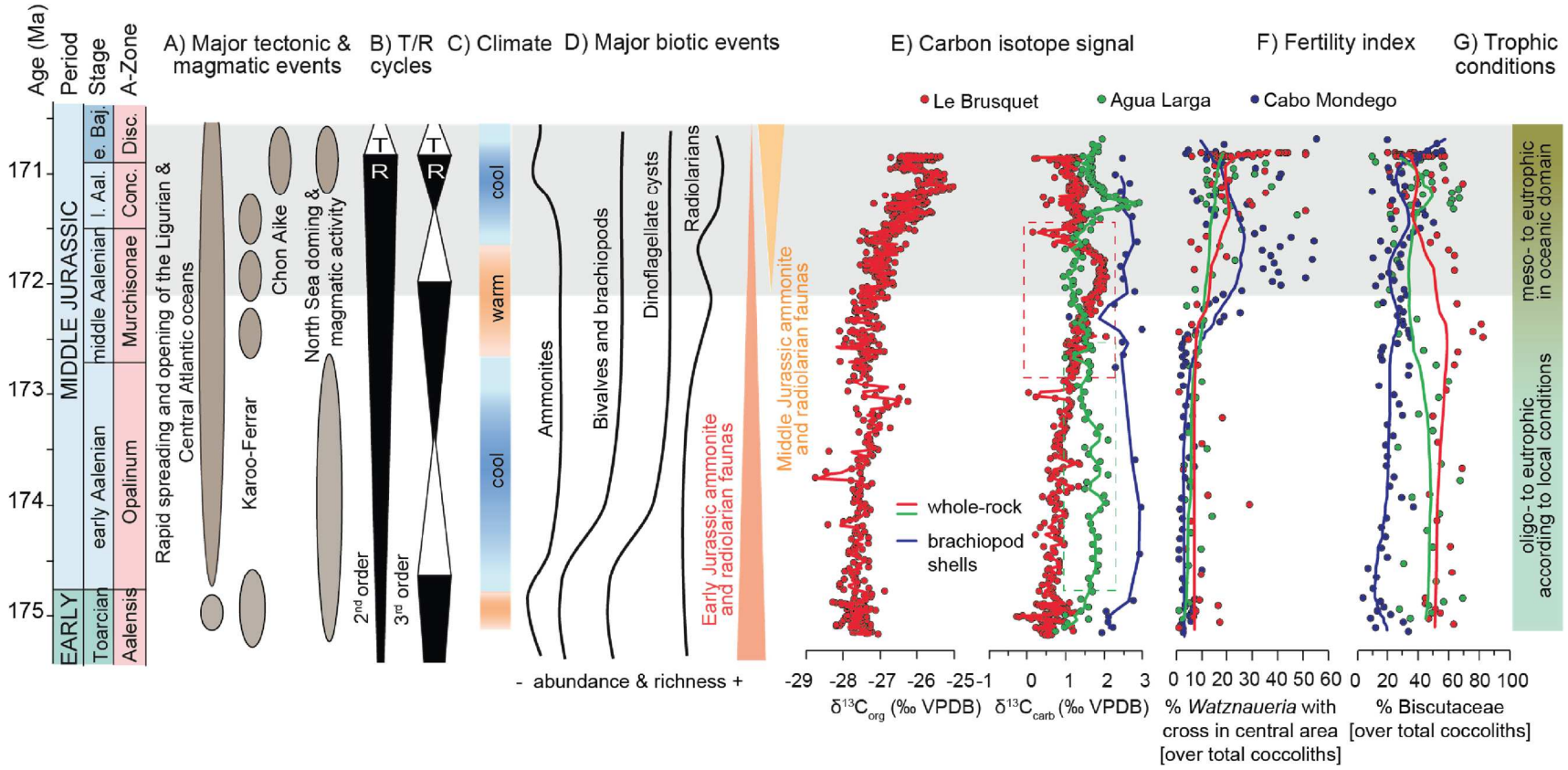

Fig. 9: Summary of key features recorded during the Aalenian time interval. **(A)** Timing of the main tectonic and magmatic events (after Dera et al., 2011 and reference therein). (B) 2nd and 3rd order transgressive (T) and regressive (R) sequences (Hardenbol et al., 1998). **(C)** Climate modes are inferred from the oxygen-isotope data from belemnites, brachiopods and bivalves (Jenkyns et al., 2002; Gomez et al., 2009; Price, 2009; Dera et al., 2011; Korte et al., 2015; Ferreira et al., 2019). **(D)** Major biotic events observed in different taxa, refer to the text for more details (Hallam, 1976; Yao, 1997; Alméras and Fauré, 2000; O'Dogherty et al., 2006; Sandoval et al., 2008; Taylor and Ernst, 2008; Wiggan, 2017). **(E)** Compilation of carbon isotopic records from Le Brusquet in France (this study), Cabo Mondego in Portugal (Ferreira et al., 2019), and Agua Larga in Spain (Sandoval et al., 2008). At Le Brusquet and Agua Larga, the box with dashed line indicates the interval where the $d^{13}C_{carb}$ signal is likely influenced by the carbonate ooze exported from adjacent platforms. The trend lines correspond to a 4-points moving average**. (F)** Fertility index refers to the percentage of *Watnaueria* and Biscutaceae from Le Brusquet (this study), Cabo Mondego (Ferreira et al., 2019) and Agua Larga (Sandoval et al., 2008). The trend lines are calculated using a LOWESS smoothing (α = 0.2) with the PAST software package (Hammer et al., 2001). **(G)** Trophic conditions are based on the proportions of *Watnaueria* and Biscutaceae. Note that the grey interval highlights the major increase in in calcareous nannofossils species indicative of fertility of oceanc water across the middle–late Aalenian.

6. Conclusions

This study provides high-resolution carbon isotope records for the Aalenian time interval and shows for the first time a record from the southern hemisphere. Consecutive medium-term $\delta^{13}C$ fluctuations expressed in different carbon sources and identified in Tethyan, Boreal, and Panthalassic sites, suggest that the Aalenian was marked by recurrent changes in the global carbon cycle. An increase in calcareous nannofossils species related to seawater fertility coincides with an episode of platform carbonate factory demise across the middle–late Aalenian, indicating that supraregional biotic and environmental changes in both pelagic and neritic environments occurred earlier than the well-known Bajocian event. The middle–late Aalenian coincided with evolutionary and ecological changes in different taxa in worldwide-distributed sites, indicating that the middle–late Aalenian was a time of palaeoceanographic and palaeoenvironmental changes. To date, there is no consensus about the triggering mechanisms leading to these palaeoenvironmental changes. Still, tectonic rearrangement and volcanic activity during the early Middle Jurassic might have potentially played an important role. There is now compelling evidence that the Aalenian was marked by recurrent global carbon cycle perturbations associated with palaeoenvironmental and palaeoceanographic changes, which likely acted as precursors of the early Bajocian event, initiating the Mesozoic Marine Revolution.

Acknowledgements

This research was funded by the Swiss National Science Foundation (project P2LAP2_181440). We express our deepest gratitude to Myette Guiomar and Didier Bert from the Reserve Géologique de Haute-Provence for providing fieldwork and sampling permits. We would like to thank Tiffany Monnier, Brahimsamba Bomou (University of Lausanne),

803 and Mickaël Charpentier for their assistance in the laboratory, Ghislaine Broillet (Université
804 Claude Bernard Lyon 1) for smear slide preparation, Paula Engell and Lasse Christiansen for
805 their help during fieldwork. We acknowledge the constructive review by James Riding and
806 Helmut Weissert. Calcareous nannofossil slides are cured at the Collections de Géologie de
807 Lyon with a FSL number.

808

809 **References**

810 Aguado, R., O'Dogherty, L., Sandoval, J., 2008. Fertility changes of surface waters during the
811 Aalenian of the Western Tethys as revealed by calcareous nannofossils and carbon
812 cycle perturbations. Marine Micropaleontology, 68, 268–285

813 Alméras, Y., Fauré, P., 2000. Les Brachiopodes liasiques des Pyrénées. Paléontologie,
814 Biostratigraphie, Paléobiogéographie et Paléoenvironnements. Strata, série 2, 10, 36-
815 39

816 Arndt, S., Jørgensen, B.B., LaRowe, D.E., Middelburg, J.J., Pancost, R.D., Regnier, P., 2013.
817 Quantifying the degradation of organic matter in marine sediments: a review and
818 synthesis. Earth Sci. Rev., 123, 53–86

819 Bartolini, A., Baumgartner, P.O., Hunziker, J.C., 1996. Middle and late Jurassic carbon
820 stable-isotope stratigraphy and radiolarite sedimentation of the Umbria-Marche Basin
821 (Central Italy). Eclogae Geol. Helv. 89, 811–844

822 Bartolini, A., Baumgartner, P.O., Guex, J., 1999. Middle and Late Jurassic radiolarian
823 palaeoecology versus carbon-isotope stratigraphy. Palaeogeography,
824 Palaeoclimatology, Palaeoecology, 145, 43–60

825 Bartolini, A., Larson, R. L., 2001. Pacific microplate and the Pangea supercontinent in the
826 Early to Middle Jurassic. Geology, 29 (8), 735-738

827 Behar, F., Beaumont, V., Penteado, H.L.D., 2001. Rock-Eval 6 technology: performances and
828 developments. Oil Gas Sci. Technol. 56 (2), 111–134

829 Bill, M., O'Dogherty, L., Guex, J., Baumgartner, P.O., 844 Masson, H., 2001. Radiolarite
830 ages in Alpine-Mediterranean ophiolites: Constraints on the oceanic spreading and the
831 Tethys-Atlantic connection. Geological Society of America Bulletin 113, 129-143

832 Bodin, S., Meissner, P., Janssen, N.M.M., Steuber, T., Mutterlose, J., 2015. Large igneous
833 provinces and organic carbon burial: Controls on global temperature and continental
834 weathering during the Early Cretaceous. Global and Planetary Change, 133, 238-253

835 Bodin, S., Krencker, F.N., Kothe, T., Hoffmann, R., Mattioli, E., Heimhofer, U., Kabiri, 2016.
836 Perturbation of the carbon cycle during the late Pliensbachian-early Toarcian: New
837 insight from high-resolution carbon isotope records in Morocco. J. Afr. Earth Sci.,
838 116, 89-104

839 Bodin, S., Hönig, M.R., Krencker, F.-N., Danish, J., Kabiri, L., 2017. Neritic carbonate crisis
840 during the Early bajocian: Divergent responses to a global environmental perturbation.
841 Palaeogeography, Palaeoclimatology, Palaeoecology, 468, 184-199

842 Bodin, S., Mau M., Sadki, D., Danisch, J., Nutz, A., Krencker, F.-N., Kabiri, L., 2020.
843 Transient and secular changes in global carbon cycling during the Bajocian event:
844 Evidence for Jurassic cool climate episodes. Global and Planetary Change, 194,
845 103287

846 Bown, P.R., 1987. Taxonomy, evolution, and biostratigraphy of Late Triassic – Early Jurassic
847 calcareous nannofossils. Palaeontol. Assoc., Spec. Pap. Palaeontol. 38. 118 pp Bown,
848 P.R., Cooper, M.K.E. 1998. Jurassic. In: Bown, P.R. (ed.) Calcareous Nannofossil
849 Biostratigraphy. British Micropalaeontological Society Publication Series. Chapman
850 & Hall, London, 34–85

851 Bown, P.R., Young, J.R. 1998. Techniques. In: Bown, 866 P.R. (ed.) Calcareous
852 Nannoplankton Biostratigraphy. British Micropalaeontological Society Publication
853 Series. Chapman & Hall, London, 16–28

854 Burtner, R.L., Warner, M.A., 1986. Relationship between illite/smectite diagenesis and
855 hydrocarbon generation in Lower Cretaceous Mowry and Skull Creek Shales of the
856 northern Rocky Mountain area. Clay Miner. 34, 390–402

857 Caloo, B., 1970. Biostratigraphie de 1'Aalénien et de la base du Bajocien dans la région de
858 Digne (Basses-Alpes, France). Comptes rendus des séances de l'Académie des
859 Sciences (D) 271, 1938–1940

860 Canales, M.L., Henriques, M.H., 2008. Foraminifera from the Aalenian and the Bajocian
861 GSSP (Middle Jurassic) of Murtinheira section (Cabo Mondego, West Portugal):
862 Biostratigraphy and paleoenvironmental implications. Marine Micropaleontology, 67,
863 155-179

864 Caruthers, A.H., Smith, P.L., Gröcke, D.R., 2013. The Pliensbachian-Toarcian (Early
865 Jurassic) extinction, a global multi-phased event. Palaeogeogr. Palaeoclimatol.
866 Palaeoecol. 386, 104–118

867 Chamley, H., 1989. Clay Sedimentology. Springer Verlag, Berlin Ciszak, R., Magné, J.,
868 Peybernès, B., 1986. Interprétation du complexe chaotique "triasique" d'Oranie
869 (Algérie occidentale) comme un olistostrome sénonien localement réinjecté dans les
870 accidents alpins. C. R. Acad. Sc. Paris, 302, 6, 357-362

871 Cobianchi, M., Erba, E., Pirini-Radrizzani, C., 1992. Evolutionary trends of calcareous
872 nannofossil genera Lotharingius and Watznaueria during the Early and Middle
873 Jurassic. Memorie di Scienze Geologiche, Padova 43, 19-25

874 Cohen, A.S., Coe, A.L., Harding, S.M., Schwark, L., 889 2004. Osmium isotope evidence for
875 the regulation of atmospheric CO2 by continental weathering. Geology, 32, 157–160

876 Corbin, J.C., 1994. Evolution géochimique du Jurassique du Sud-Est de la France: influence
877 du niveau marin et de la tectonique. Paris VI, pp. 198

878 Courtillot, V., 1994. Mass extinctions in the last 300 milliion years: one impact and seven
879 flood basalts? Isr. J. Earth Sci. 43, 255–266

880 Curry, G.B., Brunton, C.H.C., 2007. Stratigraphic distribution of brachiopods. In Selden, P.A.
881 (Ed), Treatise on Invertebrate Paleontology. Part H. Brachiopoda. Revised. Vol. 6.
882 Geological Society of America, University of Kansas, Boulder and Lawrence, 2901-
883 3081

884 de Graciansky, P.C., Dardeau, G., Dumont, T., Jacquin, T., Marchand, D., Mouterde, R., Vail,
885 P.R., 1993. Depositional sequence cycles, transgressive-regressive facies cycles, and

886 extensional tectonics: example from the southern Subalpine Jurassic basin, France.
887 Bull. Soc. Géol., France, 5, 709-718

888 De Kaenel, E., Bergen, J.A., 1993. New Early and Middle Jurassic coccolith taxa and
889 biostratigraphy from the eastern proto-Atlantic (Morocco, Portugal and DSDP Site
890 547B). Eclogae Geologicae Helvetiae 86: 861-907

891 de Lange, G.J., van Os, B., Pruysers, P.A., Middelburg, J.J., Castradori, D., Van Santvoort, P.,
892 Müller, P.J., Eggenkamp, H., Prahl, F.G., 1994. Possible early diagenetic alteration of
893 paleoproxies. In: Zahn, R. (ed.) Carbon Cycling in the Glacial Ocean: Constraints on
894 Ocean's Role in Global Climate Change. NATO ASI Series, 17, 225–258

895 Delfaud, J., Revert, J., Sabrier, R., 2000. La limite Lias–Dogger et la naissance de la
896 plateforme occitane. Strata, série 1, 10, 67-69

897 Dera, G., Brigaud, B., Monna, F., Laffont, R., Pucéat, E., Deconinck, 912 J.-F., Pellenard, P.,
898 Joachimski, M.M., Durlet, C., 2011. Climatic ups and downs in a disturbed Jurassic
899 world. Geology, 39, 3, 215-218

900 Dera, G., Toumoulin, A., De Baets, K., 2016. Diversity and morphological evolution of
901 Jurassic belemnites from South Germany. Palaeogeography, Palaeoclimatology,
902 Palaeoecology, 457, 80–97

903 Duarte, L.V., Krautter, M., Ferreira Soares, A., 2001. Bioconstructions a spongiaires siliceux
904 dans le Lias terminal du Bassin lusitanien (Portugal); stratigraphie, sedimentologie et
905 signification paleogeographique. Bull. Soc. Géol. France, 172 (5), 637-646

906 Duncan, R.A., Hooper, P.R., Rahacek, J., Marsh, J.S., Duncan, A.R., 1997. The timing and
907 duration of the Karoo igneous event, southern Gondwana. J. Geophys. Res. 102,
908 18127–18138

909 Durlet, C., Thierry, J., 2000. Modalites sequentielles de la transgression aaleno-bajocienne sur
910 le sud-est du Bassin parisien. Bull. Soc. Géol. France, 171 (3), 327-339

911 Elmi, S., Rulleau, L., 1993. Le Jurassique du Beaujolais méridional, bordure orientale du
912 Massif Central, France. GEOBIOS, 15, 139-155

913 Erba E., 2004. Calcareous nannofossils and Mesozoic oceanic anoxic events. Mar.
914 Micropaleontol., 52: 85-106. Erba, E., Gambacorta, G., Tiepolo, M., 2019. The lower

915 Bajocian Gaetani level: Lithostratigraphic marker of a potential Oceanic Anoxic
916 Event. Riv. Ital. Paleontol. Stratigr. 125, 219–230

917 Erba, E., Gambacorta, G., Tiepolo, M., 2019. The Lower Bajocian Gaetani Level:
918 Lithostratigraphic marker of a potential oceanic anoxic event. Rivista Italiana di
919 Paleontologia e Stratigrafia, 125 (1), 219-230

920 Espitalié, J., Deroo, G., Marquis, F., 1985. La pyrolyse Rock-935 Eval et ses applications;
921 première partie. Rev. Inst. Fr. Pétrol. 40, 563–579

922 Fantasia, A., Föllmi, K.B., Adatte, T., Bernárdez, E., Spangenberg, J.E., Mattioli, E., 2018.
923 The Toarcian Oceanic Anoxic Event in southwestern Gondwana: an example from the
924 Andean Basin, northern Chile. J. Geol. Soc. 175, 883–902

925 Ferreira, J., Mattioli, E., Pittet, B., Cachão, M., Spangenberg, J.E., 2015. Palaeoecological
926 insights on Toarcian and lower Aalenian calcareous nannofossils from the Lusitanian
927 Basin (Portugal). Palaeogeogr. Palaeoclimatol. Palaeoecol. 436, 245–262

928 Ferreira, J., Mattioli, E., van de Schootbrugge, B., 2017. Palaeoenvironmental vs.
929 Evolutionary control on size variation of coccoliths across the Lower-Middle Jurassic.
930 Palaeogeogr. Palaeoclimatol. Palaeoecol. 465, 177–192

931 Ferreira, J., Mattioli, E., Sucherás-Marx, B., Giraud, F., Duarte, L.D., Pittet, B., Suan, G.,
932 Hassler, A., Spangenberg, J.E., 2019. Western Tethys Early and Middle Jurassic
933 calcareous nannofossil biostratigraphy. Earth-Science Reviews, 197, 1002908

934 Ferry, S., Rubino, J.-L., 1989. Mesozoic eustacy record on western Tethyan margins. hal-
935 02013144

936 Floquet, M., Marchand, D., Sida, B. & Contini, D., 2000. Monticules micritiques à
937 spongiaires et discontinuités sédimentaires marqueurs de l'ennoiement de la
938 plateforme carbonatée de Basse Provence à l'Aalénien supérieur Bajocien inférieur.
939 In: Les événements du passage Lias-Dogger (Ed. by J. Rey & F. Ronchini). Strata, 10,
940 83-85

941 Floquet, M., Neuweiler, F., Léonide, P., 2012. The impact of depositional events and burial
942 rate on carbonate-silica diagenesis in a Middle Jurassic stromatactis carbonate mud
943 moundm Sainte-Baume Massif, SE France. Journal 957 of Sedimentary Research, 82,

944 958 521–539

945 Friedman, M., Shimada, K., Martin, L.D., Everhart, M.J., Liston, J., Maltese, A., Triebold,
946 M., 2010. 100-million-year dynasty of Giant Planktivorous bony fishes in the
947 Mesozoic seas. Science 327, 990–993

948 Gabilly, J., Cariou, E., Hantzpergue, P. 1985. Les grandes discontinuités stratigraphiques au
949 Jurassique ; témoins d'événements eustatiques, biologiques et sédimentaires. Bulletin
950 de la Société Géologique de France, 3, 391-401.

951 Gidon, M., Pairis, J.L., 1992. Relations entre le charriage de la Nappe de Digne et la structure
952 de son autochtone dans la vallée du Be s. Eclogae geol. Helv., 85/2, 327-359

953 Giraud, F., Mattioli, E., López-Otálvaro, G.E., Lécuyer, C., Suchéras-Marx, B., Alméras, Y.,
954 Martineau, F., Arnaud-Godet, F., de Kænel, E., 2016. Deciphering processes
955 controlling mid-Jurassic coccolith turnover. Mar. Micropaleontol. 125, 36–50

956 Godet, A., Bodin, S., Föllmi, K.B., Vermeulen, J., Gardin, S., Fiet, N., Adatte, T., Berner, Z.,
957 Stüben, D., Van de Schootbrugge, B., 2006. Evolution of the marine stable carbon
958 isotope record during the early cretaceous: a focus on the late Hauterivian and
959 Barremian in the Tethyan realm. Earth Planet. Sci. Lett. 242, 254–271

960 Gómez, J.J., Canales, M.L., Ureta, S., Goy, A., 2009. Palaeoclimatic and biotic changes
961 during the Aalenian (Middle Jurassic) at the southern Laurasian Seaway (Basque–
962 Cantabrian Basin, northern Spain). Palaeogeography, Palaeoclimatology,
963 Palaeoecology, 275, 14–27

964 Gorican, S., Pavsic, J., Rozic, B., 2012. Bajocian to Tithonian age of radiolarian cherts in
965 Tolmin Basin (NW Slovenia). Bull. Soc. Géol. France, 183 (4), 369-382

966 Gröschke, M., von Hillebrandt, A., Prinz, P., Quinzio, L.A. &Wilke, H.-G. 1988. Marine
967 Mesozoic paleogeography in northern Chile between 21°–26°S. In: Bahlburg, H.,
968 Breitkreuz, C. & Giese, P. (eds) The Southern Central 979 Andes. Lecture Notes in
969 Earth Sciences, 17. Springer, Berlin

970 Guinot, G., Cavin, L., 2016. 'Fish' (Actinopterygii and Elasmobranchii) diversification
971 patterns through deep time. Biol. Rev. (2016), 91, 950–981

Haccard, D., Beaudoin, B., Gigot, P., Jorda M., 1989. Notice explicative de la carte géologique de la France (1/50 000), feuille La Javie (918). – BRGM, Orléans, 152p

Hallam, A. 1976. Stratigraphic distribution and ecology of European Jurassic bivalves. Lethaia, 9, 245-249

Hammer, Ø., Harper, D.A.T., Ryan, P.D., 2001. PAST: paleontological statistics software package for education and data analysis. Palaeontologia Electronica 4, 1-9

Harazim, D., van de Schootbrugge, B., Sorichter, K., Fiebig, J.,Weug, A., Suan, G., Oschmann, W., 2013. Spatial variability of watermass conditions within three European epicontinental seaways during the Early Jurassic (Pliensbachian–Toarcian). Sedimentology 60, 359–390.

Hardenbol, J., Thierry, J., Farley, M.B., de Graciansky, P.-C., Vail, P.R., 1998. Mesozoic and Cenozoic sequence chronostratigraphic framework of European basins. In: de Graciansky, P.-C., Hardenbol, J., Jacquin, T., Vail, P.R. (Eds.), Mesozoic and Cenozoic Sequence Stratigraphy of European Basins. SEPM Spec. Publ., 60, 3–13

Hesselbo, S.P., Gröcke, D.R., Jenkyns, H.C., Bjerrum, C.J., Farrimond, P., Morgans Bell, H.S., Green, O.R., 2000. Massive dissociation of gas hydrate during a Jurassic oceanic anoxic event. Nature, 406, 392–395

Hesselbo, S.P., Morgans-Bell, H.S., McElwain, J.C., Rees, 1000 P.M., Robinson, S.A., Ross, C.E., 2003. Carbon-Cycle perturbation in the Middle Jurassic and accompanying changes in the terrestrial paleoenvironment. Journal of Geology, 111, 259–276

Jacquin, T., Dardeau, G., Durlet, C., de Graciansky, P.-C., Hantzpergue, P., 1998. The North Sea cycle: an overview of 2nd-order transgressive/regressive facies cycles in western Europe. In: de Graciansky, P.C., Hardenbol, J., Jacquin, T., Vail, P.R. (Eds.), Mesozoic and Cenozoic Sequence Stratigraphy of European Basins. SEPM Spec. Publ. 60, pp. 445–466

Jenkyns, H.C., Jones, C.E., Gröcke, D.R., Hesselbo, S.P., Parkinson, D.N., 2002. Chemostratigraphy of the Jurassic System: applications, limitations and implications for palaeoceanography. Journal of the Geological Society of London 159, 351–378

1000 Jenkyns, H.C., 2010. Geochemistry of oceanic anoxic events. Geochem. Geophys. Geosyst.
1001 11

1002 Jiang C., Chen, Z., Lavoie, D., Percival, J.B., Kabanov, P., 2017. Mineral carbon MinC(%)
1003 from Rock-Eval analysis as a reliable and cost-effective measurement of carbonate
1004 contents in shale source and reservoir rocks. Marine and Petroleum Geology, 83, 184-
1005 194

1006 Kemp, D.B., Coe, A.L., Cohen, A.S., Schwark, L., 2005. Astronomical pacing of methane
1007 release in the Early Jurassic period. Nature, 437, 396–399

1008 Kemp, D. B., Selby, D., Izumi, K., 2020. Direct coupling between carbon release and
1009 weathering during the Toarcian oceanic anoxic event. Geology, 48 (10), 976-980

1010 Korte, C., Hesselbo, S.P., Ullmann, C.V., Dietl, G., Ruhl, 1021 M., Schweigert, G., Thibault,
1011 N., 2015. Jurassic climate mode governed by ocean gateway. Nature Communications,
1012 6:10015

1013 Krencker, F.N., Bodin, S., Hofmann, R., Suan, G., Mattioli, E., Kabiri, L., Föllmi, K.B.,
1014 Immenhauser, A., 2014. The middle Toarcian cold snap: Trigger of mass extinction
1015 and carbonate factory demise. Global and Planetary Change, 117, 64-78

1016 Krencker, F.N., Lindstrom, S., Bodin, S., 2019. A major sea-level drop briefly precedes the
1017 Toarcian oceanic anoxic event: implication for Early Jurassic climate and carboncycle.
1018 Sci. Rep. 9

1019 Krencker, F.-N., Fantasia, A., Danisch, J., Martindale, R., Kabiric, L., El Ouali, M., Bodin, S.,
1020 2020. Two-phased collapse of the shallow-water carbonate factory during the
1021 latePliensbachian–Toarcian driven by changing climate and enhanced continental
1022 weathering in the Northwestern Gondwana Margin. Earth-Science Reviews, 208,
1023 103254

1024 Kump, L.R., Arthur, M.A., 1999. Interpreting carbon-isotope excursions: carbonates and
1025 organic matter. Chem. Geol. 161, 181–198

1026 Labails, C., Olivet, J.-L., Aslanian, D., Roest, W.R., 2010. An alternative early opening
1027 scenario for the Central Atlantic Ocean. Earth and Planetary Science Letters 297, 355-
1028 368

1029 Lafargue, E., Marquis, F., Pillot, D., 1997. Rock-Eval 6 Applications in Hydrocarbon
1030 Exploration, Production, And Soil Contamination Studies. Revue de l'Institut Français
1031 du Pétrole, 53, 4

1032 Lauper, B., Zimmerli, G. N., Jaeggi, D., Deplazes, G., Wohlwend, S., Rempfer, J., Foubert,
1033 A. 2021. Quantification of lithological heterogeneity within Opalinus Clay: Toward a
1034 uniform subfacies claissification scheme using a novel automated core image
1035 recognition tool. Front. Earth. Sci., 9:645596. doi: 10.3389/feart.2021.645596

1036 Léonide, P., Floquet, M., Villier, L., 2007. Interaction of 1043 tectonics, eustasy, climate and
1037 carbonate production on the sedimentary evolution of an early/middle Jurassic
1038 extensional basin (Southern Provence Sub-basin, SE France). Basin Res., 19, 125–152

1039 Le Nindre, Y.M., Manivit, J., Manivit, H., Vaslet, D., 1990. Stratigraphie séquentielle du
1040 Jurassique et du Crétacé en Arabie Saoudite. Bull. Soc. Géol. France, VI (6), 1025-
1041 1034

1042 Levert, J., 1989. Origine diagénétique complexe des minéraux argileux dans le Mésozoïque
1043 Subalpin. Geobios, mémoire special, 11, 239-251

1044 Lickorish, W.H., Ford, M., 1998. Evolution of the Digne thrust system, southern Subalpine
1045 chains: kinematics and timing of deformation. In: Mascle, A., Puigdefabregas, C.,
1046 Luterbacher, H.P., Fernandez, M. (eds) Cenozoic foreland basins of Western Europe.
1047 Geological Society, London, Special Publication, 134, 189-211

1048 López-Otálvaro, G.-E., Suchéras-Marx, B., Giraud, F., Mattioli, E., Lécuyer, C., 2012. Marine
1049 Micropaleontology, 94-95, 45-57

1050 Mattioli, E., 1996. New calcareous nannofossil species from the Early Jurassic of Tethys.
1051 Rivista Italiana di Paleontologia e Stratigrafia, 102, 397-412

1052 Mattioli, E., 1997. Nannoplankton productivity and diagenesis in the rhythmically bedded
1053 Toarcian– Aalenian Fiuminata section (Umbria– Marche Apennine, central Italy).
1054 Palaeogeogr. Palaeoclimatol. Palaeoecol. 130, 113– 133

1055 Mattioli, E., Erba, E., 1999. Biostratigraphic syntesis of calcareous nannofossil events in the
1056 Tethyan Jurassic. Rivista Italiana di Paleontologia e Stratigrafia, 105 (3), 343-376

1057 Mattioli, E., Pittet, B., Young, J.R., Bown, P.R., 2004. Biometric 1064 analysis of
1058 Pliensbachian-Toarcian (Lower Jurassic) coccoliths of the family Biscutaceae: intra-
1059 and interspecific variability versus palaeoenvironmental influence. Mar.
1060 Micropaleontol. 52, 5–27

1061 Mattioli, E., Pittet, B., 2004. Spatial and temporal distribution of calcareous nannofossils
1062 along a proximal–distal transect in the Lower Jurassic of the Umbria–Marche Basin
1063 (central Italy). Palaeogeography, Palaeoclimatology, Palaeoecology, 205, 295– 316.

1064 Mattioli, E., Pittet, B., Suan, G., Mailliot, S., 2008. Calcareous nannoplankton changes across
1065 the early Toarcian oceanic anoxic event in the western Tethys. Paleoceanograhy, 23

1066 Mariotti, N., Weis, R., Di Cencio, A., Clément, A., De Baets, K., 2012. New records of early
1067 Middle Jurassic belemnites in the French Subalpine Basin and their
1068 paleobiogeographic significance. Geobios, 45, 99-108

1069 Marticorena, L., and Tapia, I., 1982. Situacion estratigrafica del Jurasico del area de
1070 Pedernales-Quebrada Asientos. Congreso Geologico Chileno

1071 Marshall, J.D. 1992. Climatic and oceanographic isotopic signals from the carbonate rock
1072 record and their preservation. Geological Magazine, 129, 143–160

1073 McElwain, J.C., Wade-Murphy, J. & Hesselbo, S.P. 2005. Changes in carbon dioxide during
1074 an oceanic anoxic event linked to intrusion into Gondwana coals. Nature, 435, 479–
1075 482

1076 McKirdy, D. M., Powell, T. G., 1974. Metamorphic alteration of carbon isotopic composition
1077 in ancient sedimentary organic matter. New evidence from Australia and South Africa
1078 Geology, 2, 591-595

1079 Metodiev, L., 2000. Etude de la limite Toarcien–Aalénien 1086 et stratigraphie de l'Aalénien
1080 dans quelques coupes du Mont Balkan occidental et central en Bulgarie. Strata, série
1081 1, 10, 117-121

1082 Molina, J.M., Reolid, M., Mattioli, E., 2018. Thin-shelled bivalve buildup of the lower
1083 Bajocian, South Iberian paleomargin: development of opportunists after oceanic
1084 perturbations. Facies, 64, 19

1085 Morettini, E., Santantonio, M., Bartolini, A., Cecca, F., Baumgartner, P.O., Hunziker, J.C.,
1086 2002. Carbon-isotope stratigraphy and carbonate production during the Early–Middle
1087 Jurassic: examples from the Umbria–Marche–Sabina Apennines (central Italy).
1088 Palaeogeography, Palaeoclimatology, Palaeoecology, 184, 251–273

1089 Mouterde, R., Kerrien, Y., Labourguigne, J., Manivit, J., 1966. Le Lias et le Bajocien de la
1090 Javie (Basses-Alpes). Bull. Soc. Géol. De France, 7, 347-352

1091 O'Dogherty, L., Sandoval, J., Bartolini, A., Bruchez, S., Bill, M., Guex, J., 2006. Carbon
1092 isotope stratigraphy and ammonite faunal turnover for the Middle Jurassic in the
1093 Southern Iberian palaeomargin. Palaeogeography, Palaeoclimatology, Palaeoecology,
1094 239, 311–333

1095 Ohmert, W., Allia, V., C. Arias, C., Baldanza, A., Bergen, J. A., Bucefalo Palliani, R.,
1096 Canales, M. L., deKaenel, E., Garcia Joral, F., Goy, A., Herrero, C., Höhndorf, A.,
1097 Martinez, G., Mattioli, E., Perilli, N., Riegraf, W., Rolf, C., Ureta, S., Wetzel, A. &
1098 Wonik, T. 1996. Die Grenzziehung Unter-/Mitteljura (Toarcium/Aalenium) bei
1099 Wittnau und Fuentelsaz. Informationen Geologisches Landesamt Baden-
1100 Württemberg 8:1-52Pálfy, J. & Smith, P.L. 2000. Synchrony between Early Jurassic
1101 extinction, oceanic anoxic event, and the Karoo–Ferrar flood basalt volcanism.
1102 Geology, 28, 747–750

1103 Peters, K. E., 1986. Guidelines for evaluating petroleum source rock using programmed
1104 pyrolysis. Am. Assoc. Pet. Geol. Bull., 70, 318-329

1105 Pérez, E. 1982. Bioestratigrafía del Jurásico de Quebrada Asientos, norte de Potrerillos,
1106 Región de Atacama. Boletin 37. Servicio Nacional de Geología y Minería, Santiago

1107 Pittet, B., Mattioli, E., 2002. The carbonate signal and 1108 calcareous nannofossil
1108 distribution in an Upper Jurassic section (Balingen– Tieringen, Late Oxfordian,
1109 southern Germany). Palaeogeogr. Palaeoclimatol. Palaeoecol., 179, 71– 96

1110 Premoli Silva, I., Erba, E., Tornaghi, M.E., 1989. Paleoenvironmental signals and changes in
1111 surface fertility in Mid Cretaceous Corg-rich pelagic facies of the Fucoid Marls
1112 (central Italy). Géobios, Mém. Spec., 11, 225–236

1113 Price, G.D., 2010. Carbon-isotope stratigraphy and temperature change during the Early-
1114 Middle Jurassic (Toarcian-Aalenian), Raasay, Scotland, UK. Palaeogeography,
1115 Palaeoclimatology, Palaeoecology, 285, 255-263

1116 Rojas, A., Calatayud, J., Kowalewski, M., Neuman, M., Rosvall, M., 2021. A multiscale view
1117 of the Phanerozoic fossil record reveals the three major biotic transitions.
1118 Communications Biology, 4, 309

1119 Roth, P.H. 1984. Preservation of calcareous nannofossils and fine-grained carbonate particles
1120 in mid-Cretaceous sediments from the southern Angola Basin, site 530. Initial Reports
1121 of the Deep Sea Drilling Project, 75. US Government Printing Office, Washington,
1122 DC, 651–655

1123 Roth, P.H., Bowdler, J.L., 1981. Middle Cretaceous calcareous nannoplankton biogeography
1124 and oceanography of the Atlantic Ocean. Soc. Econ. Paleontol. Mineral., Spec. Publ.
1125 32, 517– 546

1126 Rousselle, B., 2001. Géologie de la «Pierre Dorée » des Monts d'Or et du Beaujolais (Rhône,
1127 France). Bulletin mensuel de la Société linnéenne de Lyon, 3, 45-60

1128 Rulleau, L., and Elmi, S. 2001. Géologie et paléontologie des dépôts ferrugineux du Toarcien
1129 et de l'Aalénien aux environs de Lyon. Travaux et Documents des Laboratoires de
1130 Géologie de Lyon, 154

1131 Sandoval, J., O'Dogherty, L., Aguado, R., Bartolini, A., Bruchez, S., Bill, M., 2008. Aalenian
1132 carbon-isotope stratigraphy: Calibration with ammonite, radiolarian and nannofossil
1133 events in the Western Tethys. Palaeogeography, Palaeoclimatology, 1131
1134 Palaeoecology, 267, 115-137.

1135 Schoell, M., 1984. Recent advances in petroleum isotope geochemistry Org. Geochem., 6,
1136 645-663

1137 Schrag, D.P., DePaolo, D.J. & Richter, F.M. 1995. Reconstructing past sea surface
1138 temperatures from oxygen isotope measurements of bulk carbonate. Geochimica et
1139 Cosmochimica Acta, 59, 2265–2278

1140 Spangenberg, J. E., Macko, S. A., 1998. Organic geochemistry of the San Vicente zinc-lead
1141 district, eastern Pucará Basin, Peru. Chemical Geology, 146, 1-23

1142 Storm, M. S., Hesselbo, S. P., Jenkyns, H. C., Ruhl, M., Ullmann, C. V., Xu, W., Leng, M. J.,
1143 Riding, J. B., Gorbanenko, O., 2020- Orbital pacing and secular evolution of the Earl
1144 Jurassic carbon cycle. Earth, Atmospheric, and Planetary Sciences, 1-9, 1912094117

1145 Suan, G., Mattioli, E., Pittet, B., Mailliot, S., Lécuyer, C., 2008a. Evidence for major
1146 environmental perturbation prior to and during the Toarcian (Early Jurassic) oceanic
1147 anoxic event from the Lusitanian Basin, Portugal. Paleoceanography 23 PA1202

1148 Suan, G., Nikitenko, B.L., Rogov, M.A., Baudin, F., Spangenberg, J.E., Knyazev, V.G.,
1149 Glinskikh, L.A., Goryacheva, A.A., Adatte, T., Riding, J.B., Föllmi, K.B., Pittet, B.,
1150 Mattioli, E., Lécuyer, C., 2011. Polar record of Early Jurassic massive carbon
1151 injection. Earth Planet. Sci. Lett., 312, 102–113

1152 Suchéras-Marx, B., Mattioli, E., Pittet, B., Escarguel, G., Suan, G., 2010. Astronomically
1153 paced coccolith size variations during the early Pliensbachian (Early Jurassic).
1154 Palaeogeogr. Palaeoclimatol. Palaeoecol., 295, 281–292

1155 Suchéras-Marx, B., Guihou, A., Giraud, F., Lécuyer, C., Allemand, 1153 P., Pittet, B.,
1156 Mattioli, E., 2012. Impact of the Middle Jurassic diversification of Watznaueria
1157 (coccolith bearing algae) on the carbon cycle and δ13C of bulk marine carbonates.
1158 Glob. Planet. Chang., 86-87, 92–100

1159 Suchéras-Marx, B., Giraud, F., Fernandez, V., Pittet, B., Lecuyer, C., Olivero, D., Mattioli,
1160 E., 2013. Duration of the early Bajocian and the associated d13C positive excursion
1161 based on cyclostratigraphy. J. Geol. Soc., 170, 107–118

1162 Suchéras-Marx, B., Mattioli, E., Giraud, F., Escarguel, G., 2015. Paleoenvironmental and
1163 paleobiological origins of coccolithophorid genus Watznaueria emergence during the
1164 late Aalenian–early Bajocian. Paleobiology, 41, 415–435

1165 Suchéras-Marx, B., Mattioli, E., Allemand, P., Giraud, F., Pittet, B., Plancq, J., Escarguel, G.,
1166 2019. The colonization of the oceans by calcifying pelagic algae. Biogeosciences, 16,
1167 2501-2510

1168 Svensen, H., Planke, S., Chevallier, L., Malthe-Sørenssen, A., Corfu, F., Jamtveit, B., 2007.
1169 Hydrothermal venting of greenhouse gases triggering Early Jurassic global warming.
1170 Earth Planet. Sci. Lett., 256, 554–566

1171 Swart, P.K., Eberli, G.P., 2005. The nature of the δ13C of periplatform sediments:
1172 Implications for stratigraphy and the global carbon cycle. Sediment. Geol., 175, 115–
1173 129

1174 Taylor, P.D., Ernst, A., 2008. Bryozoans in transition: the depauperate and patchy Jurassic
1175 biota. Palaeogeogr. Palaeoclimatol. Palaeoecol., 263, 9–23

1176 Them II, T.R., Gill, B.C., Caruthers, A.H., Gröcke, D.R., Tulsky, E.T., Martindale, R.C.,
1177 Poulton, T.P., Smith, P.L., 2017b. High-resolution carbon isotope records of the
1178 Toarcian Oceanic Anoxic Event (Early Jurassic) from 1176 North America and
1179 implications for the global drivers of the Toarcian carbon cycle. Earth Planet. Sci.
1180 Lett., 459, 118–126

1181 Thierry, J., 2000. Late Toarcian. In: Dercourt, J., Gaetani, M., Vrielynck, B., Barrier, E., Biju-
1182 Duval, B., Brunet, M.F., Cadet, J.P., Crasquin, S., Sandulescu, M. (Eds.), Atlas Peri-
1183 Tethys. Palaeogeographical Maps

1184 Tiraboschi, D., Erba, E., 2010. Calcareous nannofossil biostratigraphy (Upper Bajocian–
1185 Lower Bathonian) of the Ravin du Bès section (Bas Auran, Subalpine Basin, SE
1186 France): Evolutionary trends of Watznaueria barnesiae and new findings of
1187 "Rucinolithus" morphotypes. Geobios, 43, 59–76

1188 Tremolada, F., van de Schootbrugge, B., Erba, E., 2005. Early Jurassic schizosphaerellid
1189 crisis in Cantabria, Spain: implications for calcification rates and phytoplankton
1190 evolution across the Toarcian oceanic anoxic event. Paleoceanography, 20,
1191 doi:10.1029/2004PA001120

1192 Uliana, M.A., Bibble, K.T. & Cerdan, J. 1989. Mesozoic extension and the formation of
1193 Argentine sedimentary basins. In: Tankard, R.J.&Balkwill, H.R. (eds) Extensional
1194 Tectonics and Stratigraphy of the North Atlantic Margin. AAPG Memoirs, 46, 599–
1195 614

1196 van Breugel, Y., Baas, M., Schouten, S., Mattioli, E., Sinninghe-Damsté, J.S., 2006.
1197 Isorenieratane record in black shales from the Paris Basin, France: constraints on
1198 recycling of respired CO2 as a mechanism for negative carbon isotope shifts during
1199 the Toarcian oceanic anoxic event. Paleoceanography, 21, 1–8

1200 Vermeij, G.J., 1977. The Mesozoic marine revolution: evidence 1198 from snails, predators
1201 and grazers. Paleobiology 3, 245–258.Vicente, J.C. 2005. Dynamic paleogeography of
1202 the Jurassic Andean Basin: pattern of transgression and localisation of main straits
1203 through the magmatic arc. Revista de la Asociacion Geologica Argentina, 60, 221–250

1204 Visentin, S., Faucher, G., Mattioli, E., Erba, E., 2020. Taxonomic revision of the genus
1205 Carinolithus (Early - Middle Jurassic) based on morphometric analyses and diagenesis
1206 observations: Implications for biostratigraphy and evolutionary trends.Marine
1207 Micropaleontology, 162, 101950

1208 von Hillebrandt, A., and Schmidt-Effing, R. 1981. Ammoniten aus dem Toarcium (Jura) von
1209 Chile (Südamerika). Zitteliana, 6, 3–74

1210 von Hillebrandt, A., and Westermann, G.E.G., 1985. Aalenian (Jurassic) Ammonite Faunas
1211 and Zones of the Southern Andes. Zitteliana, 12, 3-55

1212 Watkins, D., 1986. Calcareous nannofossil paleoceanography of the Cretaceous Greenhorn
1213 Sea. Geol. Soc. Am. Bull., 97, 1239– 1249

1214 Weissert, H., McKenzie, J., Hochuli, P. 1979. Cyclic anoxic events in the Early Cretaceous.
1215 Geology, 7 (3): 147-151

1216 Wiggan, N.J., Riding, J.B., Franz, M., 2017. Resolving the Middle Jurassic dinoflagellate
1217 radiation: the palynology of the Bajocian of Swabia, Southwest Germany. Rev.
1218 Palaeobot. Palynol. 238, 55–87.Xu, W., Ruhl, M. et al. 2017. Carbon sequestration in
1219 an expanded lake system during the Toarcian oceanic anoxic event. Nature
1220 Geoscience, 10, 129–135

1221 Yao, A.,1997. Faunal change of Early–Middle Jurassic radiolarians. In: Yao, A. (Ed.),
1222 Proceedings of the Fifth Radiolarian Symposium. News of Osaka
1223 Micropaleontologists, special Volume, 10. 155–182

1224